

PUBLISHED VERSION

Guido Veit, Kathryn Oliver, Pirjo M. Apaja, Doranda Perdomo, Aurélien Bidaud-Meynard, Sheng-Ting Lin, Jingyu Guo, Mert Icyuz, Eric J. Sorscher, John L. Hartman IV, Gergely L. Lukacs
Ribosomal stalk protein silencing partially corrects the $\Delta F508$ -CFTR functional expression defect
PLoS Biology, 2016; 14(5):e1002462-1-e1002462-32

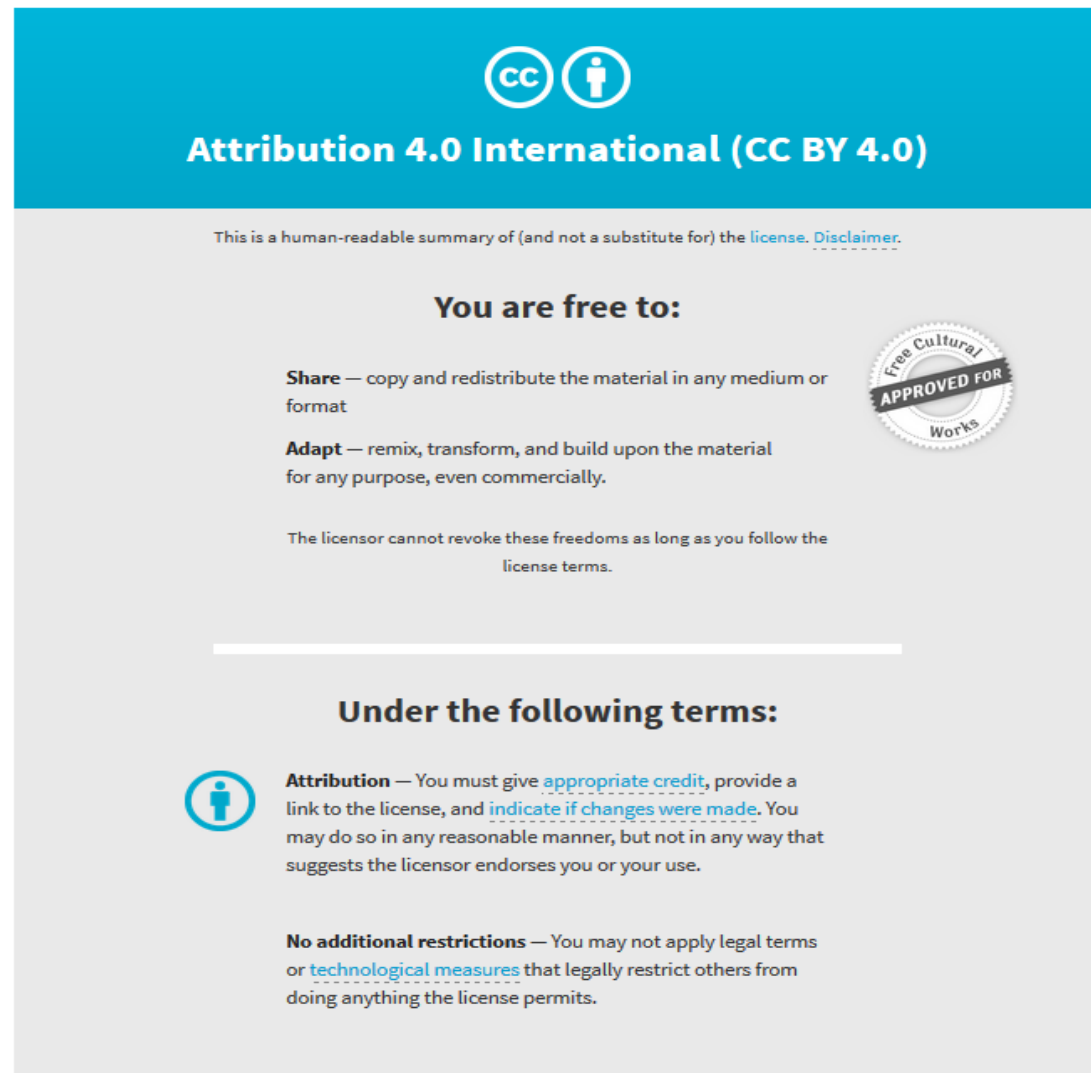
Copyright: © 2016 Veit et al. This is an open access article distributed under the terms of the Creative Commons Attribution License, which permits unrestricted use, distribution, and reproduction in any medium, provided the original author and source are credited

Originally published at:

<http://doi.org/10.1371/journal.pbio.1002462>

PERMISSIONS

<http://creativecommons.org/licenses/by/4.0/>



The image shows the Creative Commons Attribution 4.0 International License banner. It features the CC logo and a person icon in a circle. The text reads: "Attribution 4.0 International (CC BY 4.0)". Below this, it states: "This is a human-readable summary of (and not a substitute for) the [license](#). [Disclaimer](#)." The main section is titled "You are free to:" and lists two freedoms: "Share" (copy and redistribute) and "Adapt" (remix, transform, and build upon). A circular seal on the right says "Free Cultural APPROVED FOR Works". Below this, it notes: "The licensor cannot revoke these freedoms as long as you follow the license terms." The next section is titled "Under the following terms:" and lists two conditions: "Attribution" (give appropriate credit, provide a link to the license, and indicate if changes were made) and "No additional restrictions" (do not apply legal terms or technological measures that restrict others).

7 November 2017

<http://hdl.handle.net/2440/107869>

RESEARCH ARTICLE

Ribosomal Stalk Protein Silencing Partially Corrects the $\Delta F508$ -CFTR Functional Expression Defect

Guido Veit¹, Kathryn Oliver^{2,3}, Pirjo M. Apaja¹, Doranda Perdomo¹, Aurélien Bidaud-Meynard¹, Sheng-Ting Lin¹, Jingyu Guo², Mert Icyuz², Eric J. Sorscher⁴, John L. Hartman IV^{2,3*}, Gergely L. Lukacs^{1,5,6*}

1 Department of Physiology, McGill University, Montréal, Quebec, Canada, **2** Department of Genetics, University of Alabama at Birmingham, Birmingham, Alabama, United States of America, **3** Gregory Fleming James Cystic Fibrosis Research Center, University of Alabama at Birmingham, Birmingham, Alabama, United States of America, **4** Department of Pediatrics, Emory University School of Medicine, Atlanta, Georgia, United States of America, **5** Department of Biochemistry, McGill University, Montréal, Quebec, Canada, **6** Groupe de Recherche Axé sur la Structure des Protéines (GRASP), McGill University, Montréal, Quebec, Canada

* jhartman@uab.edu (JLH); gergely.lukacs@mcgill.ca (GLL)



CrossMark
click for updates

OPEN ACCESS

Citation: Veit G, Oliver K, Apaja PM, Perdomo D, Bidaud-Meynard A, Lin S-T, et al. (2016) Ribosomal Stalk Protein Silencing Partially Corrects the $\Delta F508$ -CFTR Functional Expression Defect. *PLoS Biol* 14 (5): e1002462. doi:10.1371/journal.pbio.1002462

Academic Editor: David Ron, University of Cambridge, UNITED KINGDOM

Received: November 17, 2015

Accepted: April 14, 2016

Published: May 11, 2016

Copyright: © 2016 Veit et al. This is an open access article distributed under the terms of the [Creative Commons Attribution License](https://creativecommons.org/licenses/by/4.0/), which permits unrestricted use, distribution, and reproduction in any medium, provided the original author and source are credited.

Data Availability Statement: All relevant data are within the paper and its Supporting Information files.

Funding: This work was supported by Howard Huges Medical Institute (www.hhmi.org) Physician-Scientist Early Career Award P/S ECA 57005927 and Cystic Fibrosis Foundation (www.cff.org) Research Grant MILLER08G0 to JLH, the Cystic Fibrosis Foundation R464-CR11 and National Institutes of Health (NIH) - National Institute of Diabetes and Digestive and Kidney Diseases (NIDDK, www.nidk.nih.gov) P30DK072482 to EJS, NIH-NIDDK R01DK75302, Cystic Fibrosis Canada (www.cysticfibrosis.ca) and Canadian Institutes of Health

Abstract

The most common cystic fibrosis (CF) causing mutation, deletion of phenylalanine 508 ($\Delta F508$ or Phe508del), results in functional expression defect of the CF transmembrane conductance regulator (CFTR) at the apical plasma membrane (PM) of secretory epithelia, which is attributed to the degradation of the misfolded channel at the endoplasmic reticulum (ER). Deletion of phenylalanine 670 ($\Delta F670$) in the yeast oligomycin resistance 1 gene (*YOR1*, an ABC transporter) of *Saccharomyces cerevisiae* phenocopies the $\Delta F508$ -CFTR folding and trafficking defects. Genome-wide phenotypic (phenomic) analysis of the Yor1- $\Delta F670$ biogenesis identified several modifier genes of mRNA processing and translation, which conferred oligomycin resistance to yeast. Silencing of orthologues of these candidate genes enhanced the $\Delta F508$ -CFTR functional expression at the apical PM in human CF bronchial epithelia. Although knockdown of *RPL12*, a component of the ribosomal stalk, attenuated the translational elongation rate, it increased the folding efficiency as well as the conformational stability of the $\Delta F508$ -CFTR, manifesting in 3-fold augmented PM density and function of the mutant. Combination of *RPL12* knockdown with the corrector drug, VX-809 (lumacaftor) restored the mutant function to ~50% of the wild-type channel in primary *CFTR* ^{$\Delta F508/\Delta F508$} human bronchial epithelia. These results and the observation that silencing of other ribosomal stalk proteins partially rescue the loss-of-function phenotype of $\Delta F508$ -CFTR suggest that the ribosomal stalk modulates the folding efficiency of the mutant and is a potential therapeutic target for correction of the $\Delta F508$ -CFTR folding defect.

Research (www.cihr-irsc.gc.ca) to GLL. GLL is a Canada Research Chair (www.chairs-chaires.gc.ca). The funders had no role in study design, data collection and analysis, decision to publish, or preparation of the manuscript.

Competing Interests: JLH is founder and holds equity in Spectrum PhenomX LLC, which holds a license from the University of Alabama at Birmingham to commercialize Q-HTCP technology. The authors declare no other competing interests.

Abbreviations: ABC, ATP-binding cassette; ABCC, ATP-binding cassette family C; BCA, bichoninic acid; CF, cystic fibrosis; CFTR, cystic fibrosis transmembrane conductance regulator; CFTRc, Cystic Fibrosis Translational Research center; CHX, cycloheximide; cpt-cAMP, 8-(4-Chlorophenylthio)-adenosine-3',5'-cyclic monophosphate; Frk, forskolin; FRT, Fisher rat thyroid; GAC, GTPase-associated center; gen, genistein; GO, gene ontology; hERG, human Ether-à-go-go-Related Gene; IBMX, 3-Isobutyl-1-methyl-xanthine; Inh₁₇₂, inhibitor 172; I_{sc}, short-circuit current; KEGG, Kyoto Encyclopedia of Genes and Genomes; MLC1, megalencephalic leukoencephalopathy with subcortical cyst 1; NBD1, nucleotide binding domain 1; NT, nontargeted; PKA, protein kinase A; PM, plasma membrane; Q-HTCP, quantitative high throughput cell array phenotyping; r $\Delta F508$, low-temperature rescued $\Delta F508$ -CFTR; SGA, synthetic genetic array; SP_PIR, SwissProt—Protein Information Resource; TfR, transferrin receptor; V2R, vasopressin 2 receptor; YOR1, yeast oligomycin resistance 1.

Author Summary

Cystic fibrosis (CF) is one of the most common autosomal recessive diseases in Caucasians. It is caused by mutations in the CF transmembrane conductance regulator (CFTR), which functions as an anion channel at the apical plasma membrane of secretory epithelia. The most common CF mutation, a deletion of the phenylalanine residue at position 508 ($\Delta F508$), results in the channel misfolding and subsequent intracellular degradation. Our previous genome-wide phenotypic screens, using a yeast variant, have predicted modifier genes for $\Delta F508$ -CFTR biogenesis. Here, we show that silencing of one of these candidate genes, *RPL12*, a component of the ribosomal stalk, increased the folding and stabilization of $\Delta F508$ -CFTR, resulting in its increased plasma membrane expression and function. Our data suggest that reducing the translational elongation rate via *RPL12* silencing can partially reverse the $\Delta F508$ -CFTR folding defect. Importantly, *RPL12* silencing in combination with the corrector drug VX-809 (lumacaftor), increased the mutant function to 50% of the wild-type CFTR channel, suggesting that the ribosomal stalk perturbation may represent a therapeutic target for rescuing the $\Delta F508$ -CFTR biogenesis defect.

Introduction

Cystic fibrosis (CF), caused by mutations in cystic fibrosis transmembrane conductance regulator (CFTR), is characterized by multiorgan pathology, mainly affecting the upper and lower airways, gastrointestinal tract, and endocrine system [1,2]. To date ~2,000 mutations have been identified in the *CFTR* gene with widely variable disease severity [3–5]. The gene product, CFTR, is an ATP-binding cassette (ABC) transporter, which functions as a cyclic AMP-regulated chloride and bicarbonate channel in secretory epithelia [2,6]. Deletion of the phenylalanine at position 508 (Phe508del, designated as $\Delta F508$) in the nucleotide binding domain 1 (NBD1), the most common CF-causing mutation, results in misfolding and premature degradation of the mutant via the endoplasmic reticulum (ER)-associated degradation pathway (ERAD) [7–9]. The small amount of $\Delta F508$ -CFTR molecules that escape the ER are functionally, conformationally, and biochemically unstable and are rapidly removed from the plasma membrane (PM) via the endolysosomal associated degradation pathway [10,11].

To rescue the folding defect of $\Delta F508$ -CFTR, several strategies have been pursued with limited success so far [12–14]. Small molecule correctors that act as pharmacological chaperones, like VX-809, can directly bind to and promote the folding of $\Delta F508$ -CFTR [15–19]. In combination with the gating potentiator VX-770, VX-809 achieved only modest benefit in CF patients homozygous for the $\Delta F508$ mutation [20], which might be attributed in part to the destabilization of $\Delta F508$ -CFTR upon chronic exposure to VX-770 [21,22]. Modifier genes may also facilitate the $\Delta F508$ -CFTR functional rescue by enhancing the mRNA or protein expression, folding, stability, or by inhibiting its degradation at the ER and post-ER compartments [11,12, 23–25]. Candidate modifier genes have been isolated by genome-wide SNP studies [26,27], identification of the CFTR interactome [28–30], and phenotypic screens of targeted siRNA libraries [11,31]. As a complementary approach, strategies focusing on reverting the maladaptive stress response in CF have been proposed [32]. None of these approaches, however, appear to attain sufficient functional correction in preclinical studies to be therapeutically robust in patients with the most common CF mutation, particularly in individuals carrying only one copy of $\Delta F508$ -CFTR, representing 40% of US CF patients [3].

Chimeras between the yeast ABC transporter STE6 and $\Delta F508$ -CFTR were used as a homology model to identify revertant mutations [33], but these chimeras are not recognized by the

ER quality control [34]. Recently, we have employed a genome-wide screen to identify modifiers of CFTR misfolding, utilizing high-throughput yeast phenomic analysis of Yor1, a member of the ABC transporter superfamily, with deletion of phenylalanine 670 (Yor1- Δ F670). The Δ F508-equivalent mutation, Yor1- Δ F670, results in protein misfolding, ER retention, and proteasomal degradation similar to that of Δ F508-CFTR in mammalian cells [35–37]. Oligomycin, which inhibits the ATP synthase, is extruded by Yor1 across the PM, enabling a screen of the yeast gene deletion strain library [37,38] for modulators of Yor1- Δ F670 processing as determined by oligomycin sensitivity. Our phenomic screen provided a comprehensive gene interaction network that can potentially modulate Δ F508-CFTR biogenesis [39]. Evolutionary conservation in the Δ F-biogenesis network was demonstrated by the identification of many yeast homologs of published human genes that modulate Δ F508-CFTR biogenesis similarly to that of Yor1- Δ F670 function [39].

Here, we validated a subset of genes that were identified by quantitative high throughput cell array phenotyping (Q-HTCP) in the yeast model, including components of the cytoplasmic exosome, rRNA biogenesis pathway, and most notably, the ribosomal stalk, in human respiratory cells. We show that silencing of ribosomal stalk proteins, in particular *RPL12*, increases the rescued Δ F508-CFTR PM density, function, and thermal stability, suggesting that ribosomal stalk proteins have a determinant role in the folding of the mutant channel and may represent a possible therapeutic target for correction of the Δ F508-CFTR folding defect. Furthermore, the results highlight the capacity of yeast phenomic screen as a systematic approach to investigate disease modifier genes, adding CF to a list of human diseases where yeast can function as a powerful model system [40–42].

Results

Phenomic Analysis Reveals Evolutionarily Conserved Gene Interaction Modules That Influence Yor1- Δ F670 Function

To select hits from our previous yeast screen [39] for further study in human cells, the top 180 gene deletions that increased oligomycin resistance of Yor1- Δ F670-associated oligomycin sensitivity (or deletion suppressors) were prioritized by retesting and secondary screening with additional experimental controls (described below). The hits were also subjected to analysis by the DAVID bioinformatics tool [43]. Functional annotation clustering identified two groups, ribosomal or ribosome-associated genes and genes involved in RNA degradation, with an enrichment score of > 2 (S1A Fig). These analyses revealed several gene interaction modules (e.g. multiple subunits of a protein complex) and, when analyzed in parallel with the *yor1- Δ 0* (null) allele, verified that oligomycin resistance required interaction with Yor1- Δ F670 (Fig 1). Additionally, Yor1- Δ F670 interactions were confirmed by expressing the protein from a different promoter and without the C-terminal GFP fusion, that was used in our original screen. Double mutants were remade in quadruplicate using modified synthetic genetic array (SGA) methodology [44,45], and the new panel of double mutants was subjected to Q-HTCP to obtain growth curves at multiple oligomycin concentrations [37]. Growth curves were fit to a logistic growth function, and gene interaction was measured with respect to the cell proliferation parameter, *L* (Fig 1A), which corresponds to the time at which a culture reaches half of the carrying capacity [46]. Multiple components of the cytoplasmic exosome (*SKI2*, *SKI3*, *SKI7*) (Figs 1C and S1B), genes involved in ribosomal RNA processing and the nuclear exosome (*LRP1*, *RRP6*, and *RRP8*) (Figs 1D and S1B), and ribosomal structural proteins (*RPL12A*, *RPP2B*, *RPS7A*, and *RPL19A*) (Figs 1B, 1E and S1B) were identified based on increased resistance to oligomycin upon the gene deletion, in the context of Yor1- Δ F670, but not *yor1- Δ 0* (Fig 1). On this basis, we focused on the cytoplasmic and nuclear exosome,

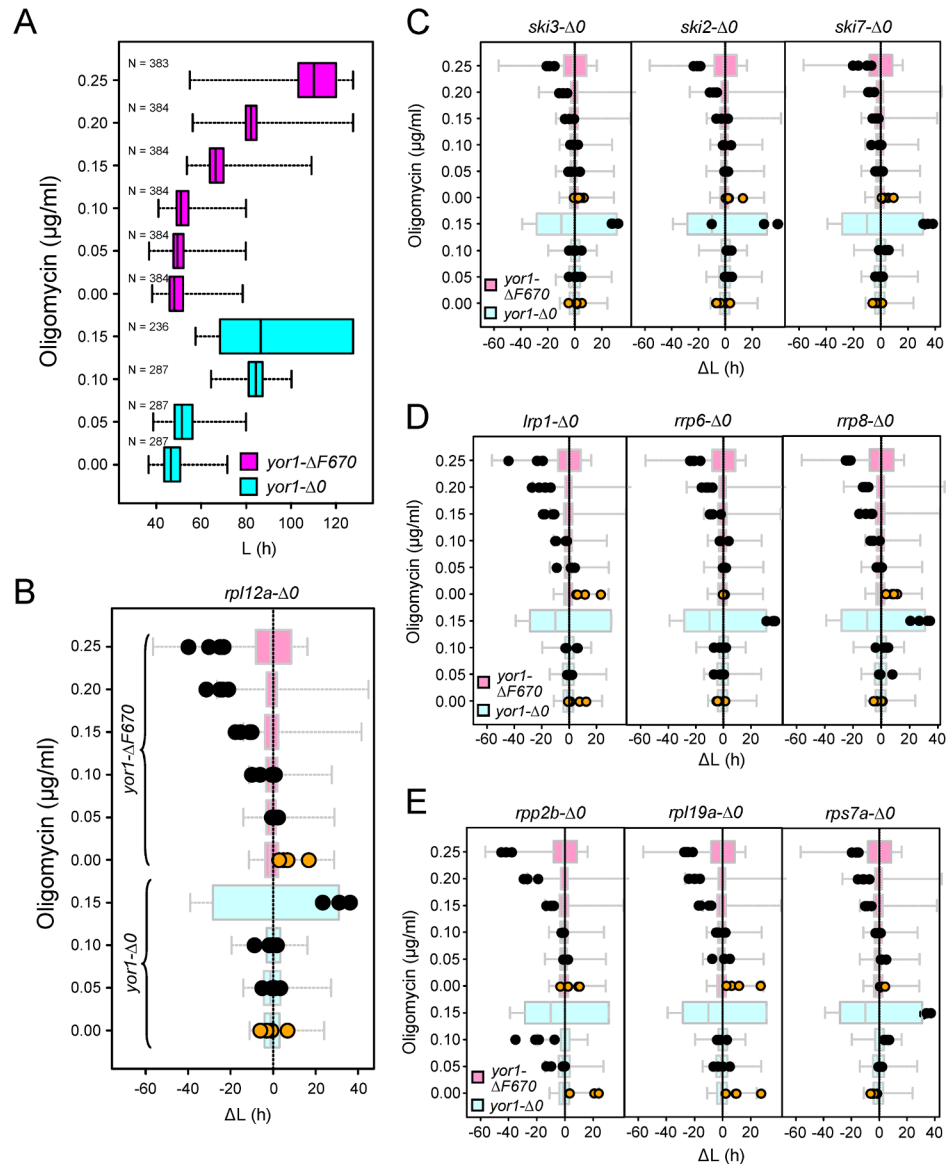


Fig 1. Genes involved in the function of the cytoplasmic exosome, nuclear exosome, rRNA processing and ribosome influence the function of Yor1- $\Delta F670$. (A) Box-whisker plot of the cell proliferation parameter L (time to reach half-maximal carrying capacity) of the *yor1- ΔO* (gene deletion) strain (cyan) and the *yor1- $\Delta F670$* mutant (magenta) following treatment with oligomycin at multiple concentrations. 287 cultures were analyzed for *yor1- ΔO* and 384 cultures for *yor1- $\Delta F670$* . “N < 287” or “N < 384” indicates that the concentration of oligomycin was fully growth inhibitory for some of the replicate cultures. Box plots indicate the central 75% of values, whiskers the total value range and averages are indicated by black bars. At higher growth inhibitory concentrations, the phenotypic distributions widen, and thus the high range for the *yor1- ΔO* at 0.15 $\mu\text{g/ml}$ oligomycin is not depicted to permit better visualization of the data. The single mutant reference strain data from panel A is dose-normalized and plotted in the background for the identically normalized double-mutant data (black dots) in panels B–E to illustrate how each gene deletion influences the oligomycin resistance associated with the *yor1- ΔO* and *yor1- ΔF* alleles. (B) The *RPL12A* deletion increases oligomycin resistance in the context of *yor1- $\Delta F670$* (magenta), but not *yor1- ΔO* (cyan). Oligomycin resistance was compared between the single mutants (shown in panel A) and the respective double mutant cultures, separately constructed in quadruplicate (biological replicates, black circles). Data for each series of replicates was normalized by the difference in L in the absence of oligomycin (orange circles). (C–E) Plots similar to those in panel B are shown for gene modules comprising the cytoplasmic exosome involved in mRNA regulation (C), genes functioning in the nuclear exosome and rRNA processing (D), and additional ribosomal proteins (E). See [Table 1](#) for additional information. The underlying data of panels A–E can be found in [S1 Data](#).

doi:10.1371/journal.pbio.1002462.g001

Table 1. Yeast deletion suppressors of Yor1- Δ F670 grouped by functional module with human homologs and functional annotations.

Yeast gene	Human gene	Human UniProt ID	Yeast functional annotation
<i>SKI2</i>	<i>SKIV2L</i>	Q15477	Ski complex component and putative RNA helicase; mediates 3'→5' RNA degradation by the cytoplasmic exosome
<i>SKI3</i>	<i>TTC37</i>	Q6PGP7	Ski complex component and TPR protein; mediates 3'→5' RNA degradation by the cytoplasmic exosome
<i>SKI7</i>			Coupling protein that mediates interactions between the Ski complex and the cytoplasmic exosome
<i>LRP1</i>			Nuclear exosome-associated nucleic acid binding protein
<i>RRP6</i>	<i>EXOSC10</i>	Q01780	Nuclear exosome exonuclease component
<i>RRP8</i>	<i>HUCE1</i>	O43159	Nucleolar S-adenosylmethionine-dependent rRNA methyltransferase
<i>RPL12A</i>	<i>RPL12</i>	P30050	Component of 60S ribosomal subunit stalk
<i>RPP2B</i>	<i>RPLP2</i>	P05387	Component of 60S ribosomal subunit stalk
<i>RPL19A</i>	<i>RPL19</i>	P84098	Component of 60S ribosomal subunit
<i>RPS7A</i>	<i>RPS7</i>	P62081	Component of 40S ribosomal subunit

doi:10.1371/journal.pbio.1002462.t001

ribosomal RNA biogenesis, and ribosomal proteins in order to test for the evolutionarily conserved influence of their knockdown on Δ F508-CFTR biogenesis in mammalian cells ([Table 1](#)).

Silencing Human Homologs of Yeast Yor1- Δ F670 Biogenesis Modifier Genes Similarly Influences PM Expression of Δ F508-CFTR

To test for functional conservation among human homologs of *S. cerevisiae* genes found to regulate Yor1- Δ F670 biogenesis, we used the human CF bronchial epithelial CFBE41o- (or CFBE) cell line with *CFTR*^{*AF508/AF508*} genetic background with no detectable CFTR protein expression as a model [47]. CFBE cells were engineered to express inducible WT- and/or Δ F508-CFTR-3HA as described [17,48]. As an indirect measure of biogenesis and/or peripheral stability of Δ F508-CFTR, first the PM density of the mutant channel was determined by cell surface ELISA in polarized CFBE after siRNA-mediated knockdown of the putative target genes. Two or three nonoverlapping siRNA sequences were used individually for each candidate gene to discriminate possible off-target effects. SiRNA silencing of Yor1- Δ F modifier homologs increased the PM density of the low-temperature (26°C) rescued Δ F508-CFTR (r Δ F508-CFTR) by up to ~3-fold, representing ~8% of the WT CFTR PM density, similar to the level achieved by the FDA-approved corrector, VX-809 ([Fig 2A](#)). A 50% increase in the PM density of r Δ F508-CFTR for at least two siRNAs in comparison to nontargeted (NT) siRNA were considered as criteria for further investigation. These were met by siRNA-mediated silencing of *SKIV2L* (*SKI2* in *S. cerevisiae*), *TTC37* (*SKI3*), *EXOSC10* (*RRP6*), *RPL12* (*RPL12A*), *POMP* (*UMP1*), and *TBC1D22B* (*GYP1*) ([Fig 2A](#)).

To determine whether the biochemical rescue of r Δ F508-CFTR correlates with a gain-of-function phenotype, the PM conductance of CFBE cells was measured by the halide-sensitive YFP quenching assay in CFBE cells stably expressing the halide-sensitive YFP-H148Q/I152L/F46L, using a fluorescence plate reader [19]. The iodide influx-mediated YFP quenching was determined after maximal activation of the temperature r Δ F508-CFTR with cAMP-dependent protein kinase A (PKA) agonists forskolin (Frk), 3-Isobutyl-1-methyl-xanthine (IBMX), and 8-(4-Chlorophenylthio)-adenosine-3',5'-cyclic monophosphate (cpt-cAMP) in combination with the potentiator genistein (gen) ([Fig 2B](#)). Induction of r Δ F508-CFTR expression strongly increased the halide conductance of CFBE epithelia that was further augmented by knockdown of some of the Yor1- Δ F modifier gene homologs ([Figs 2B, 2C, S2A and S2B](#)). Knockdown of

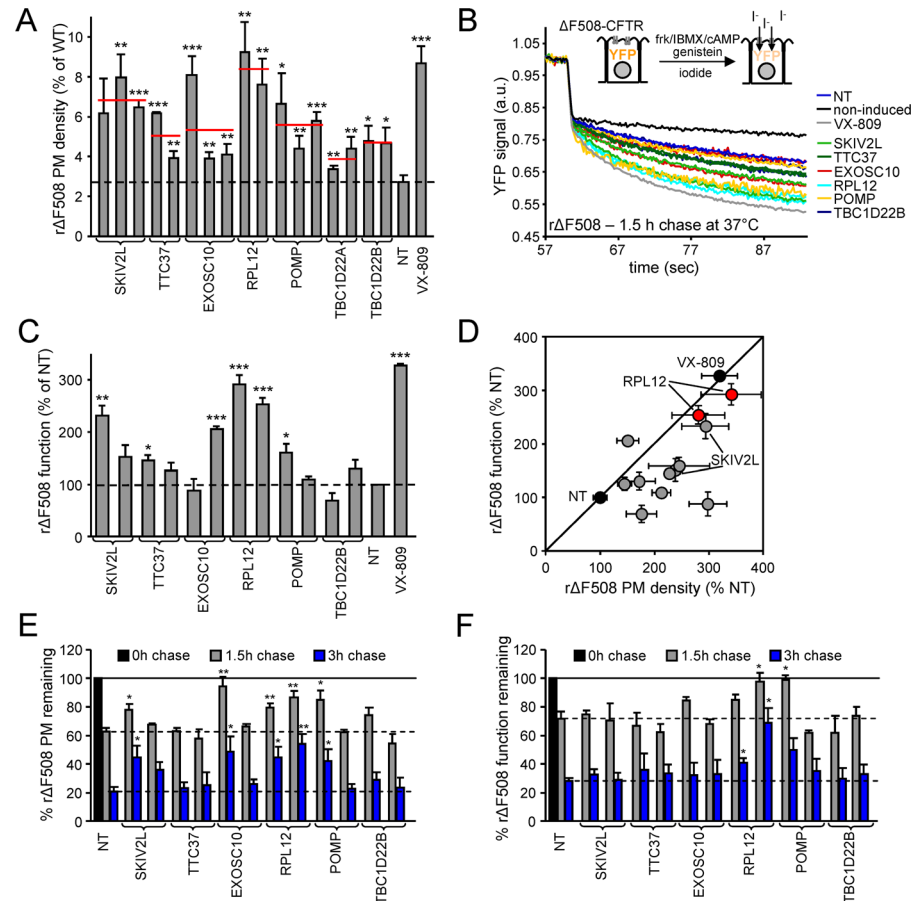


Fig 2. Knockdown of the human homologs of Yor1- $\Delta F670$ modifier genes increases the biochemical and functional expression and stability of the low temperature rescued $\Delta F508$ -CFTR. (A) PM density of r $\Delta F508$ -CFTR (48 h, 26°C) after 1 h chase at 37°C was determined by cell surface ELISA in human CFBE, expressing CFTR under the control of tetracycline inducible transactivator and is expressed as percent of wild-type (WT) CFTR. Indicated genes were silenced with two or three individual siRNAs, and the average PM density is shown as red line. NT siRNA served as negative and the corrector VX-809 as positive controls ($n = 3-6$). (B) Schematic depiction of the assay (upper panel) and representative traces (lower panel) of r $\Delta F508$ -CFTR function assayed by halide-sensitive YFP quenching in CFBE cells. Knockdown was achieved with two individual siRNAs per indicated gene, and the measurement was performed after 1.5 h chase at 37°C. The $\Delta F508$ -CFTR function was measured by determining the YFP quenching kinetics in response to extracellular iodide addition in the presence of forskolin (10 μM), IBMX (250 μM), cpt-cAMP (250 μM), and genistein (50 μM). (C) The effect of the indicated gene knockdown on the function of r $\Delta F508$ -CFTR after 1.5 h chase at 37°C as determined by halide-sensitive YFP quenching ($n = 3$). (D) Correlation between the PM density and functional increase of r $\Delta F508$ -CFTR after knockdown of Yor1- $\Delta F670$ modifier homologs as determined in panels A and C. (E, F) The effect of knockdown with two individual siRNAs per gene on PM stability (E, $n = 4$) and functional stability (F, $n = 3$) of r $\Delta F508$ -CFTR after 1.5 and 3 h chase at 37°C. * $p < 0.05$, ** $p < 0.01$, *** $p < 0.001$. Error bars indicate standard error of the mean (SEM) of 3–6 independent experiments. The underlying data of panels A, C, E, and F can be found in [S1 Data](#).

doi:10.1371/journal.pbio.1002462.g002

RPL12 or *SKIV2L*, by two independent siRNAs, increased the mutant channel PM function by >50%. Notable, *RPL12* knockdown induced ~270% transport activity of the NT control (Fig 2C).

RPL12 knockdown, similar to VX-809, proportionally increased the PM density and function of r $\Delta F508$ -CFTR (Fig 2D). In contrast, silencing of *SKIV2L* and most of the other genes tested, evoked a more substantial gain in PM density in comparison to function, suggesting the preferential escape of partially folded, poorly functional $\Delta F508$ -CFTR molecules from the ER

(Fig 2D). The inference that *RPL12* knockdown enhanced the r $\Delta F508$ -CFTR conformational stability was supported by measuring the PM turnover of r $\Delta F508$ -CFTR. The r $\Delta F508$ -CFTR removal from the PM was ~5-fold faster ($T_{1/2}$ ~2 h) in comparison to its WT counterpart ($T_{1/2}$ of >10 h) after exposure to 37°C, which can be attributed to the channel unfolding, reflected by its increased protease susceptibility and ubiquitination that largely accounts for the accelerated internalization, lysosomal targeting, and attenuated recycling [11,49]. *RPL12* knockdown considerably slowed down the r $\Delta F508$ -CFTR biochemical and functional turnover at the PM (Fig 2E and Fig 2F). Jointly, these observations suggest that *RPL12* deficiency promotes r $\Delta F508$ -CFTR functional PM expression by facilitating the biogenesis and enhancing peripheral stability of the mutant.

Considering that the modifier genes of the Yor1- ΔF -CFTR processing defect can contribute to the regulation of translation, RNA processing, and vesicle transport, we tested the possibility that silencing of *TBC1D22B*, *RPL12*, *EXOSC10*, *SKIV2L*, *POMP*, or *TTC37* genes can alter the cellular expression of native and conformationally defective membrane proteins in general. Ablation of these genes, however, did not increase the Ca^{2+} -activated TMEM16A Cl⁻ channel activity, nor the transferrin receptor (TfR) or the conformationally defective, mutant megalencephalic leukoencephalopathy with subcortical cyst 1 (MLC1-S280L) PM densities, as determined by the halide-sensitive YFP quenching assay [48], transferrin-HRP binding, or cell surface density measurement of MLC1-S280L, respectively (S2C–S2E Fig). Thus, silencing of these Yor1- ΔF deletion suppressor proteins does not universally influence PM protein biogenesis.

siRNA-Mediated Knockdown of *RPL12* Increases the Expression of Functional $\Delta F508$ -CFTR at the Cell Surface

To examine the effects of *RPL12* silencing at physiological temperature, the $\Delta F508$ -CFTR function at the PM was studied in polarized CFBE monolayers. Both siRNAs decreased the *RPL12* protein and mRNA expression by ~50% and ~40%, respectively (S3A and S3B Fig). In parallel, the $\Delta F508$ -CFTR PM density was increased by 2.5–5-fold relative to the NT siRNA treated cells (Fig 3A). The $\Delta F508$ -CFTR PM density was comparably augmented in nonpolarized HeLa cells, suggesting that the *RPL12* knockdown effect is not CFBE-specific and independent of CFTR polarized expression (S3C Fig). *RPL12* knockdown also enhanced the PM density of WT-CFTR in CFBE and HeLa cells (Figs 3A and S3C), probably by increasing the limited maturation efficiency of the WT channel [17,50].

To distinguish whether *RPL12* knockdown promotes the accumulation of the mature, complex-glycosylated (band C) $\Delta F508$ -CFTR in post-ER compartments, or causes the channel redistribution from intracellular pools to the PM, the expression level of complex-glycosylated $\Delta F508$ -CFTR was determined by immunoblot (IB) analysis. Since we were unable to visualize the complex-glycosylated form in the inducible CFBE expression system (Fig 3B), these experiments were also performed in CFBE cells constitutively expressing the channel at higher level, while preserving the hallmarks of $\Delta F508$ -CFTR misprocessing (CFBE^C) [51,52]. In this model, the *RPL12* knockdown increased the abundance of the complex-glycosylated $\Delta F508$ -CFTR (Fig 3C). Interestingly, *RPL12* knockdown led to the steady-state accumulation of the core-glycosylated $\Delta F508$ -CFTR (band B) as well (Fig 3B and Fig 3C).

In accord with the increased PM expression, *RPL12* silencing augmented the halide conductance (Fig 3D) and the Frk-stimulated short-circuit current (I_{sc}) by up to 5-fold (Fig 3E). This was further enhanced by addition of the potentiator gen in the constitutive $\Delta F508$ -CFTR expressors (Fig 3E). In contrast, *RPL12* knockdown had little effect on the function of WT-CFTR in CFBE (S3D Fig).

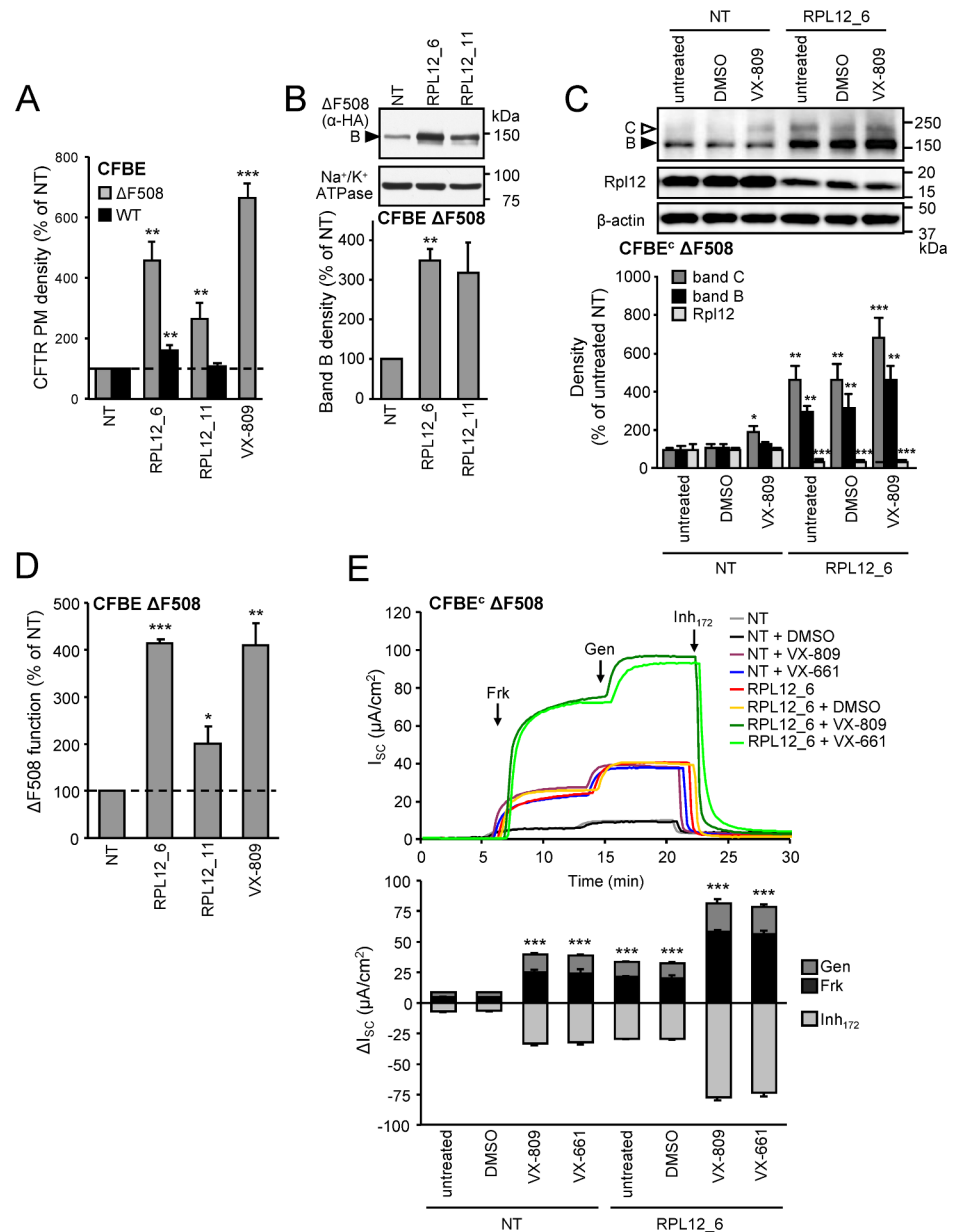


Fig 3. SiRNA-mediated silencing of *RPL12* increases $\Delta F508$ -CFTR expression, PM density and function at 37°C. (A) PM density of WT and $\Delta F508$ -CFTR upon *RPL12* knockdown in CFBE at 37°C ($n = 3$). (B) Effect of *RPL12* knockdown on the expression pattern of $\Delta F508$ -CFTR determined by immunoblotting in CFBE (upper panel). CFTR was visualized using anti-HA antibody, anti- Na^+/K^+ -ATPase served as loading control. Densitometric analysis (lower panel, $n = 3$) of the core-glycosylated (band B, filled arrowhead) $\Delta F508$ -CFTR is expressed as percent of controls transfected with NT siRNA ($n = 3$). (C) The effect of *RPL12* knockdown, VX-809 treatment (3 μM , 24 h) or combination of both on the expression pattern of $\Delta F508$ -CFTR expressed constitutively in CFBE cells (CFBE^c). Immunoblots (upper panel) were probed with antibodies against CFTR (10B6.2), Rpl12, and β -actin as a loading control. Expression levels of Rpl12 and the core- (band B, filled arrowhead) or complex-glycosylated (band C, empty arrowhead) $\Delta F508$ -CFTR were quantified by densitometry and are expressed as a percentage compared to controls transfected with NT siRNA (lower panel, $n = 3$). (D) *RPL12* knockdown increases the function of $\Delta F508$ -CFTR at physiologic temperature as determined by halide sensitive YFP quenching assay ($n = 3$). (E) Representative short-circuit current (I_{sc}) recordings (upper panel) and quantification of the changes (ΔI_{sc} , $n = 5$, lower panel) in CFBE^c monolayers expressing $\Delta F508$ -CFTR after siRNA-mediated *RPL12* knockdown or NT siRNA transfection. CFTR mediated currents were induced by sequential acute addition of Frk (10 μM) and gen (50 μM) followed by CFTR inhibition with inhibitor₁₇₂ (10 μM) in the presence of a basolateral-to-apical chloride gradient after

basolateral permeabilization with amphotericin B (100 μ M). The values in D and E were normalized to account for the increase in Δ F508-CFTR mRNA upon siRPL12_6 treatment. * $p < 0.05$; ** $p < 0.01$; *** $p < 0.001$. Error bars show SEM of 3–5 independent experiments. The underlying data of panels A–E can be found in [S1 Data](#).

doi:10.1371/journal.pbio.1002462.g003

RPL12 Knockdown and VX-809 Additively Increase the Functional Expression of Δ F508-CFTR in Immortalized and Primary Human Bronchial Epithelia

To confirm the relevance of *RPL12* silencing on the rescue of Δ F508-CFTR misprocessing, we used primary human bronchial epithelia (HBE) isolated from five CF patients with *CFTR* ^{Δ F508/ Δ F508} genotype. CF-HBE were cultured on permeable filter supports at air–liquid interface for 3 wk and transfected with either NT or RPL12_6 siRNA every 7 d, resulting in a decrease of Rpl12 protein expression by \sim 25% ([Fig 4A](#)). Alternatively, RPL12 silencing was achieved by a single transfection with a double-stranded Dicer-substrate siRNA [53] ([S4A Fig](#)). The chronic knockdown of *RPL12* did not alter tight junction formation, the differentiation of goblet and ciliated cells and the development of transepithelial resistance of the monolayers ([S4D Fig and S4E Fig](#)).

The effect of *RPL12* siRNA alone or in combination with VX-809 was determined on Frk plus gen-activated and inhibitor 172 (Inh₁₇₂)-sensitive I_{sc} of Δ F508-CFTR in CFBE and CF-HBE. VX-809-mediated Δ F508-CFTR correction was additive with *RPL12* knockdown, increasing the maximal I_{sc} to \sim 50% of WT-CFTR in CFBE ([Figs 3E and S3D](#)). As expected, a large variation of the I_{sc} was observed in CF-HBE cells from individual patients ([Figs 4B, 4C, S4B and S4C](#)). *RPL12* silencing enhanced the PKA-activated current by a mean \sim 2.2-fold (range 1.1–3.1-fold) in the presence of the potentiator gen. This corresponds to \sim 35.7% of the WT-CFTR current, measured in HBE isolated from non-CF lungs ([Figs 4C, S3E and S4C](#)). VX-809 treatment alone increased the Δ F508-CFTR current by \sim 2.1-fold (range 1.6–2.7-fold), representing \sim 27.7% of the WT-CFTR current as observed before [54] ([Figs 4C, S3E and S4C](#)). Combination of *RPL12* knockdown with VX-809 treatment augmented the Frk- and gen-stimulated I_{sc} by \sim 4.0 fold (range 3.1–4.9-fold), representing 54.4% of WT-CFTR in HBE cells ([Figs 4C, S3E and S4C](#)).

RPL12 knockdown also increased the amount of complex-glycosylated Δ F508-CFTR in HBE, similar to that in CFBE ([Fig 4A](#)). Treatment with VX-809 alone led to \sim 2-fold enhanced expression of the complex-glycosylated form in both CFBE and CF-HBE cells. The rescue effect of VX-809 was at least doubled upon *RPL12* silencing, indicated by \sim 6- and \sim 4-fold increase of the band C abundance of Δ F508-CFTR in CFBE and HBE, respectively ([Figs 3C and 4A](#)). These findings support the notion that distinct mechanisms are responsible for the *RPL12* knockdown-mediated rescue and VX-809-dependent correction of the Δ F508-CFTR functional expression defect in both CFBE and HBE cells.

RPL12 Knockdown Increases the Δ F508-CFTR Folding Efficiency at the ER

We postulated that *RPL12* knockdown may enhance the conformational maturation efficiency of non-native Δ F508-CFTR at the ER and/or stabilize the native-like conformation of the mutant, delaying its cell surface removal. The low folding efficiency of the nascent Δ F508-CFTR chains were measured by the conversion efficiency of the core-glycosylated Δ F508-CFTR into complex-glycosylated form during an extended radioactive pulse labeling (3 h) and chase (2 h) at 37°C. To measure the total [³⁵S]-methionine and [³⁵S]-cysteine incorporation during the pulse, while minimizing the degradation of core-glycosylated forms, the pulse duration was reduced to 30 and 20 min in parallel samples of CFBE and HeLa cells,

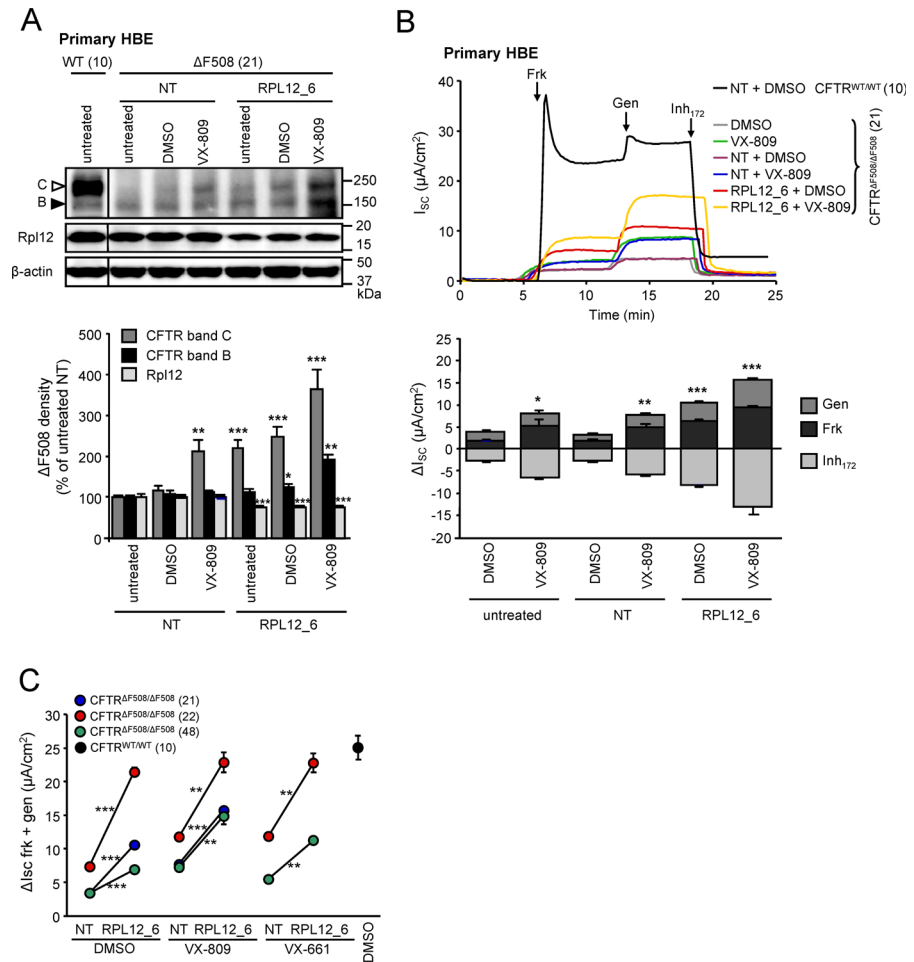


Fig 4. *RPL12* knockdown is additive with VX-809 in primary CF human bronchial epithelia (HBE). (A) The effect of *RPL12* knockdown, VX-809 treatment (3 μ M, 24 h) or combination of both on the expression pattern of endogenous $\Delta F508$ -CFTR in HBE cells isolated from one CF patient with *CFTR* ^{$\Delta F508/\Delta F508$} genotype (upper panel, patient code 21). Immunoblots were probed with antibodies against CFTR (1:1 mixture of UNC antibodies 570 and 596), Rpl12, and β -actin as a loading control. Expression levels of Rpl12 and the core- (band B, filled arrowhead) or complex-glycosylated (band C, open arrowhead) $\Delta F508$ -CFTR were quantified by densitometry and are depicted as a percentage compared to controls transfected with NT siRNA (lower panel, $n = 3$). (B) Representative I_{sc} recordings (upper panel) and quantification of the changes (ΔI_{sc} , lower panel) after siRNA-mediated *RPL12* knockdown, NT siRNA or mock transfection in HBE cells homozygous for $\Delta F508$ -CFTR (patient code 21, $n = 3$). A representative I_{sc} trace of HBE with *CFTR*^{WT/WT} genotype is shown for comparison (upper panel). (C) Quantification of the Frk- and gen-stimulated current (ΔI_{sc} Frk + gen) in HBE isolated from three different homozygous $\Delta F508$ CF patients (21, 22, and 48) or one WT-CFTR donor (10) transfected with *RPL12_6* or NT siRNA for 21 days alone or in combination with VX-809 (3 μ M, 24 h) (C) and VX-661 (3 μ M, 24 h). CFTR mediated currents were induced by sequential acute addition of Frk (10 μ M) and gen (50 μ M) followed by CFTR inhibition with inhibitor 172 (*Inh*₁₇₂, 10 μ M) in the presence of a basolateral-to-apical chloride gradient. * $p < 0.05$; ** $p < 0.01$; *** $p < 0.001$. Error bars show SEM of three independent experiments. The underlying data of panels A–C can be found in [S1 Data](#).

doi:10.1371/journal.pbio.1002462.g004

respectively, (Fig 5A). *RPL12* knockdown increased the $\Delta F508$ -CFTR ER folding efficiency from ~1.9% to ~3.2% in CFBE and from ~1.4 to ~4.4% in HeLa cells (Fig 5A and Fig 5B), while it decreased the radioactive labeling of the core-glycosylated $\Delta F508$ -CFTR by 50–80% both at 26°C and 37°C (Fig 5A–5C) without reducing the CFTR transcript level (S5A Fig). We obtained similar results by using a shorter pulse-labeling time (10 min) (S5C Fig). Combination of *RPL12* knockdown with VX-809 additively increased the $\Delta F508$ -CFTR maturation

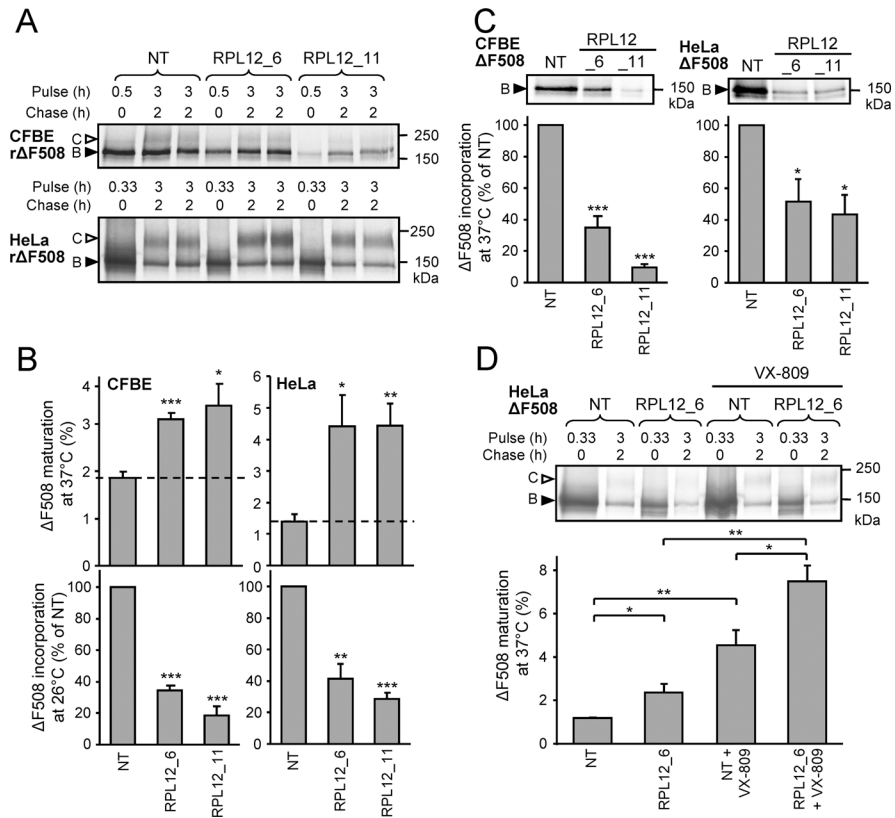


Fig 5. *RPL12* knockdown increases the conformational maturation of Δ F508-CFTR at the ER. (A) Determination of Δ F508-CFTR translation and ER folding efficiency by metabolic pulse chase in CFBE and HeLa cells transfected with *RPL12* or NT siRNA. Labeling with [³⁵S]-methionine and [³⁵S]-cysteine was performed to measure translation (30 min in CFBE or 20 min in HeLa at 26°C) or maturation efficiency (for 3 h at 26°C followed by 2 h chase at 37°C) in duplicates. **(B)** The folding efficiency of Δ F508-CFTR after 2 h chase at 37°C in CFBE (left upper panel) and HeLa cells (right upper panel) was determined by calculating the percent of pulse-labeled immature, core-glycosylated Δ F508-CFTR (B-band, filled arrowhead in A) conversion into the mature, complex-glycosylated form (C-band, empty arrowhead in A) ($n = 4-6$). The total labeling for 3 h was extrapolated from values obtained for 20 or 30 min pulse labeled samples. Quantitative analysis of ³⁵S-methionine and ³⁵S-cysteine incorporation during the 20 or 30 min labeling period at 26°C into the newly formed Δ F508-CFTR in CFBE (left lower panel) and HeLa cells (right lower panel) ($n = 3$). **(C)** [³⁵S]-methionine and [³⁵S]-cysteine incorporation during the labeling period at 37°C into the newly formed Δ F508-CFTR in CFBE (left panel, 30 min) and HeLa cells (right panel, 20 min) ($n = 3$). **(D)** Determination of Δ F508-CFTR translation and ER folding efficiency by metabolic pulse chase in HeLa cells transfected with *RPL12* or NT siRNA with or without VX-809. Labeling was performed for 20 min with no chase (0 h chase) or for 3 h followed by 2 h chase, both at 37°C. The folding efficiency of Δ F508-CFTR after 2 h chase at 37°C is depicted in the lower panel ($n = 3$) and was calculated based on the extrapolated total labeling for 3 h from values obtained for the 20 min pulse labeled samples without chase. Radioactivity was quantified based on phosphorimage analyses and not by densitometry of the autoradiographs used for illustration. * $p < 0.05$, ** $p < 0.01$, *** $p < 0.001$. Error bars show SEM of 3–6 independent experiments. The underlying data of panels B–D can be found in [S1 Data](#).

doi:10.1371/journal.pbio.1002462.g005

efficiency from 4.5% to ~7.5% relative to that in the presence of VX-809 alone, at 37°C ([Fig 5D](#)), consistent with nonoverlapping mechanisms of action.

RPL12 Silencing Cannot Indiscriminately Rescue the Processing Defect of PM Proteins

Selectivity of the *RPL12* knockdown effect was determined by measuring its impact on the cell surface density and turnover of a panel of PM proteins as surrogate readouts of their

conformational stability [11,50,55,56]. We chose mutations in the vasopressin 2 receptor (V2R-Y128S) [56,57], MLC1-P92S and -S280L [58], and the human Ether-à-go-go-Related Gene (hERG-G601S) [55], which cause diabetes insipidus (V2R), megalencephalic leukoencephalopathy (MLC1), and long QT type 2 syndrome (hERG), respectively, due to conformational defects, misprocessing and accelerated PM turnover of the respective membrane proteins [55–60].

Silencing of *RPL12* had no significant effect on PM density and stability of the V2R-Y128S and MLC-P92S or -S280L in HeLa cells (Figs 6A, 6B, S6A and S6B). In contrast, knockdown of *RPL12* increased the WT-hERG (~125% of NT) and hERG-G601S (140% of NT) PM densities (Fig 6C), without stabilizing the channels at the PM (S6C Fig). The effect on steady-state PM density of WT and mutant hERG may be due to their inefficient conformational maturation, estimated to be ~40% and ~15% determined by metabolic pulse chase experiments [61] (Fig 6E). *RPL12* knockdown increased the hERG-G601S maturation efficiency from ~15% to ~25% (Fig 6E).

Notably, incorporation of radioactive amino acids into newly synthesised hERG-G601S was decreased in *RPL12* knockdown cells (Fig 6F). This could be attributed to translational inhibition rather than cotranslational degradation, since the amount of core-glycosylated hERG was increased after a 3 h chase at 37°C (Fig 6E). The PM density of the TfR, a type I transmembrane protein [56], was only modestly decreased by *RPL12* knockdown (Fig 6D). These results support the hypothesis that the *RPL12* knockdown can preferentially influence the folding efficiency of metastable, multidomain membrane proteins.

RPL12 Silencing Enables the Biogenesis of Native-Like Δ F508-CFTR

Compelling evidence indicates that synonymous mutations can influence the folding of polypeptide via defining the available time frame for the cotranslational folding and unfolding during translation in vivo and in vitro [62–65]. If translational elongation slow down can shift the folding equilibrium of newly synthesized multidomain Δ F508-CFTR towards the WT-CFTR conformer by kinetic or thermodynamic means, it is predicted that the thermostability of complex-glycosylated mutant would be increased as compared to the temperature r Δ F508-CFTR.

The conformational stability of CFTR channels was measured by determining the thermal denaturation temperature, which induced 50% ($T_{50\%}$) conversion of detergent solubilised CFTR into SDS-resistant aggregates [66]. Cell lysates, obtained from r Δ F508 or WT CFTR CFBE expressors were heat-denatured at 20°C–80°C and the aggregation resistant, complex-glycosylated CFTR pool was quantified by immunoblotting. *RPL12* knockdown increased the $T_{50\%}$ of the complex-glycosylated r Δ F508-CFTR from ~58°C to 67°C, a value that is close to the $T_{50\%}$ of WT-CFTR (Fig 7A and Fig 7B). This observation suggests that *RPL12* silencing promotes the accumulation of conformationally more stable complex-glycosylated r Δ F508-CFTR, conceivably by shifting the mutant folding energetic towards the WT, an inference substantiated by increased metabolic stability of the r Δ F508-CFTR, determined by CHX chase and immunoblotting in HeLa cells (Fig 7C and Fig 7D). *RPL12* silencing also delayed the r Δ F508-CFTR biochemical and functional turnover at the PM in CFBE, as determined by cell surface ELISA and halide-sensitive YFP assays (Fig 7F and Fig 7G).

Surprisingly, *RPL12* knockdown delayed the turnover of the immature Δ F508-CFTR. The core-glycosylated form $T_{1/2}$ was decreased from ~30 to ~50 min in HeLa and CFBE measured by CHX chase and immunoblotting. (Figs 7C, 7E and S5D). Comparable results were obtained by the metabolic pulse-chase technique. After 2 h chase ~14% of the initially labeled immature Δ F508-CFTR remained in the *RPL12* knockdown CFBE cells as compared to ~7% in the NT control at 37°C (Fig 7H). Thus, impeded degradation of the core-glycosylated form may contribute to the enhanced ER maturation of Δ F508-CFTR in CFBE cells (see also Fig 3B and 3C).

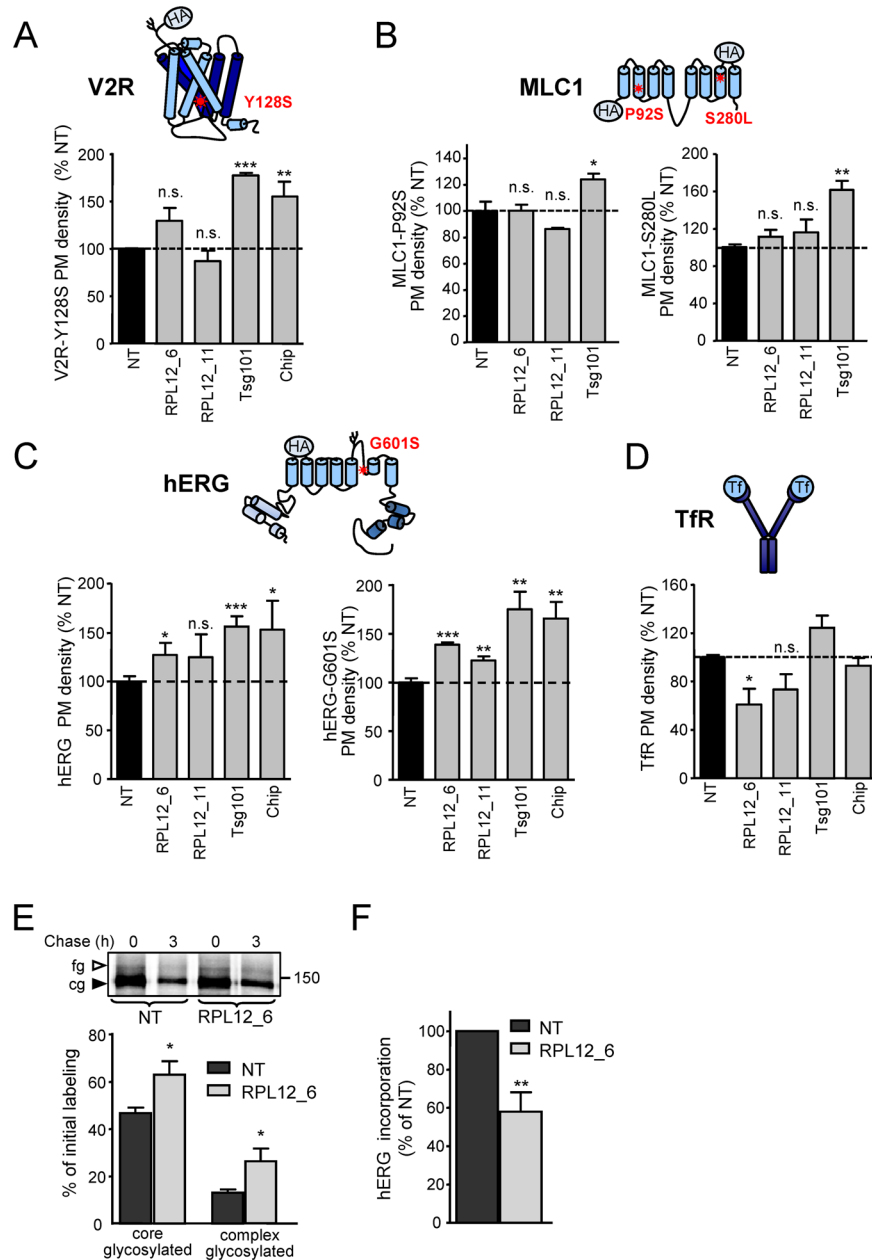


Fig 6. RPL12 knockdown increases the maturation efficiency of some misfolded membrane proteins.

(A–D) PM densities of the indicated proteins were measured by cell surface ELISA in NT or *RPL12* siRNA transfected HeLa cells. In A–C, cells stably expressing extracellular HA-epitope tagged V2R-Y128S (A, $n = 3$), MLC1-P92S and S280L (B, $n = 3$) or hERG-WT and G601S (C, $n = 4$) were used. The endogenous TfR was labeled with biotin-Tf and detected with neutravidin-HRP (D, $n = 3$). SiRNAs for CHIP and Tsg101 served as positive controls that attenuated degradation of misfolded PM proteins from post-Golgi compartments. (E) The maturation efficiency of hERG-G601S was determined by metabolic pulse chase experiment using ^{35}S -methionine and ^{35}S -cysteine in HeLa cells transfected with *RPL12* or NT siRNAs. Pulse labeling was performed for 20 min at 26°C, followed by 3 h chase at 37°C. The maturation efficiency of the channel was calculated based on the percent conversion of the pulse labeled core-glycosylated form (cg-form, filled arrowhead) into the complex-glycosylated form (fg, empty arrow head) of hERG-G601S after 3 h of chase ($n = 4$). (F) ^{35}S -methionine and ^{35}S -cysteine incorporation into newly synthesized hERG-G601S during the 20 min pulse labeling at 26°C ($n = 4$). * $p < 0.05$; ** $p < 0.01$; *** $p < 0.001$. Error bars show SEM of 3–4 independent experiments. The underlying data of panels A–F can be found in [S1 Data](#).

doi:10.1371/journal.pbio.1002462.g006

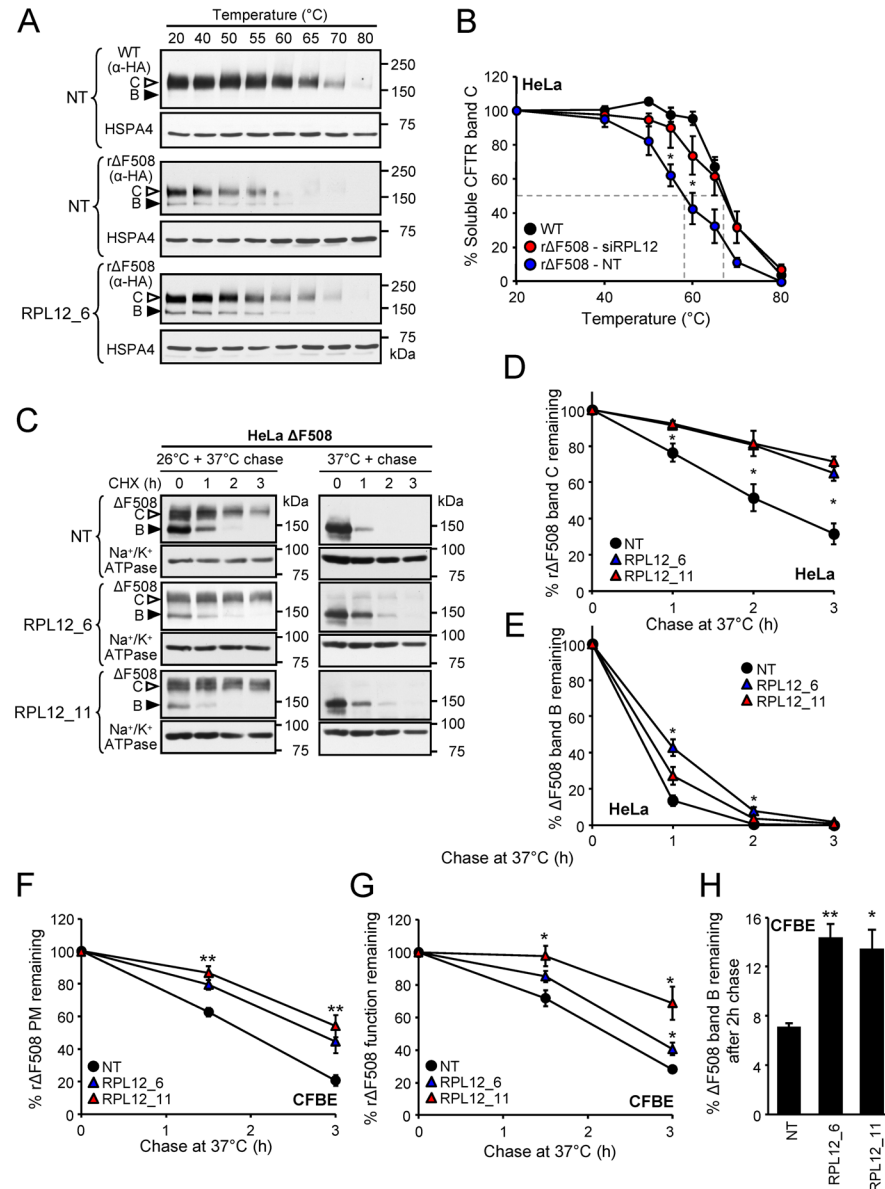


Fig 7. *RPL12* knockdown increases the stability of the core- and complex-glycosylated forms of Δ F508-CFTR. (A, B) *RPL12* ablation increases the conformational stability of the solubilised r Δ F508-CFTR. The thermoaggregation propensity of r Δ F508-CFTR as a surrogate indicator of the channel conformational stability was determined in cell lysates of HeLa cells transfected with *RPL12* or NT siRNA in comparison to WT-CFTR. To minimize the amount of core-glycosylated form (filled arrowhead), cells were treated with CHX (2 h, 100 μ g/ml) prior to lysis. Cell lysates were incubated for 15 min at 20°C–80°C followed by the sedimentation of aggregates and visualizing the remaining soluble channels by immunoblotting (A). The complex-glycosylated channel (empty arrowhead) was quantified by densitometry (B, $n = 3-5$). (C) Stability of Δ F508-CFTR after (left panel) or without (right panel) low-temperature rescue in HeLa cells upon *RPL12* knockdown was determined by immunoblot with CHX chase. (D, E) The complex-glycosylated (D, open arrowhead in C) or core-glycosylated CFTR (E, filled arrowhead in C) disappearance was quantified by densitometry and is expressed as percent of the initial amount ($n = 3$). (F, G) The effect of *RPL12* silencing on the PM stability (F, $n = 4$) and functional stability (G, $n = 3$) of r Δ F508-CFTR after 1.5 and 3 h chase at 37°C. Same values as in Fig 2E and 2F depicted as chase time-dependent percent remaining. (G) The effect of *RPL12* knockdown on the stability of metabolically labeled core-glycosylated Δ F508-CFTR in CFBE. Labeling was performed for 3 h at 26°C followed by chase for 2 h at 37°C. * $p < 0.05$; ** $p < 0.01$; *** $p < 0.001$. Error bars show SEM of 3–5 independent experiments. The underlying data of panels B and D–H can be found in S1 Data.

doi:10.1371/journal.pbio.1002462.g007

Collectively, these observations suggest that the increased folding propensity of $\Delta F508$ -CFTR in the presence of *RPL12* down-regulation account for the increased PM density, function, biochemical, and functional stability, as well as reduced potentiator-dependent fractional activation of the I_{sc} carried by $\Delta F508$ -CFTR ([S5C Fig](#) and [S5D Fig](#)).

Slow-Down of Translational Elongation Rate by Multiple Means Partially Reverts the Folding and Processing Defects of $\Delta F508$ -CFTR

RPL12 knockdown causes translational elongation slow down in yeast [67,68]. Consistently, the reduced pulse labeling of $\Delta F508$ -CFTR and HERG-G601S suggested that *RPL12* silencing may also impede the translational elongation rate in eukaryotes ([Figs 5B, 5C, 6F and 5C](#)). Due to insufficient radioactive signal incorporation into the $\Delta F508$ -CFTR nascent chain in CFBE cells, we monitored the global kinetics of run-off elongation [69] in HeLa cells after *RPL12* silencing. To this end, translation initiation was inhibited with harringtonine [70]. Then run-off elongation was measured in the presence of [35 S]-methionine and [35 S]-cysteine and terminated with cycloheximide (CHX) [71] after 1–3 min ([Fig 8A](#)). Quantification of radioactive nascent chains synthesis by phosphorimage analysis showed a considerable reduction in the global translational elongation rate in *RPL12* knockdown cells ([Fig 8B](#)). Importantly, slowing down global translational elongation in Fisher rat thyroid (FRT) cells by low concentration of CHX also induced the accumulation of the complex-glycosylated $\Delta F508$ -CFTR and partial restoration of the PM chloride conductance [72].

To confirm that pharmacological inhibition of translational elongation can partially rescue $\Delta F508$ -CFTR processing in CFBE cells, we used low-concentrations CHX or emetine. Both translational elongation inhibitors elicited a dose-dependent increase in the PM density of $\Delta F508$ -CFTR, which correlated with the decreased expression of the core-glycosylated form as a consequence of partial translational inhibition ([Fig 8C and Fig 8D](#)). These results confirmed and extended previous observations [72], suggesting that the channel folding is favoured at a slower translational elongation rate regardless of whether it is achieved by pharmacological [72] or genetic means as shown by *RPL12* ablation ([Fig 8B](#)).

siRNA-Mediated Silencing of Ribosomal Stalk Proteins or the Elongation Factor 2 Increases the Functional Expression and Stability of $\Delta F508$ -CFTR

Deletion of the *RPL12A* and *RPL12B* genes in yeast leads to a defective assembly of the ribosomal stalk, disrupting the normal stoichiometry of P1 and P2 isoforms, which along with P0, and the 26S (28S in humans) rRNA, interact with Rpl12 to form the GTPase-associated center (GAC) [67,73,74]. The stalk has been shown to participate in the translocation mechanism and to bind the eukaryotic elongation factor 2 (eEF-2), leading to the hypothesis that P-proteins act as GTPase-activators in conjunction with eEF-2 to increase the translational elongation rate [74–77]. To support the notion that compromised integrity of the ribosomal stalk could increase the functional expression of $\Delta F508$ -CFTR, the expression levels of P0 (RPLP0), P1 (RPLP1), P2 (RPLP2), and eEF-2 proteins were reduced by siRNA-mediated knockdown in CFBE. Two or three siRNA sequences were used for each gene, reducing the mRNA expression by ~10%–60% after 5 d in polarized CFBE ([S7A–S7D Fig](#)). Transfection of these siRNAs increased the PM density and function of r $\Delta F508$ -CFTR by up to 5-fold as compared to NT siRNA and indicated a good correlation between the knockdown efficiencies and the gain of PM density and function of the mutant ([Figs 9A, 9B, S7F and S7G](#)). Importantly, P0, P1, P2, and eEF2 knockdown conformationally stabilized the mutant, as indicated by the slower biochemical and functional PM turnover of the r $\Delta F508$ -CFTR ([Fig 9C and Fig 9D](#)).

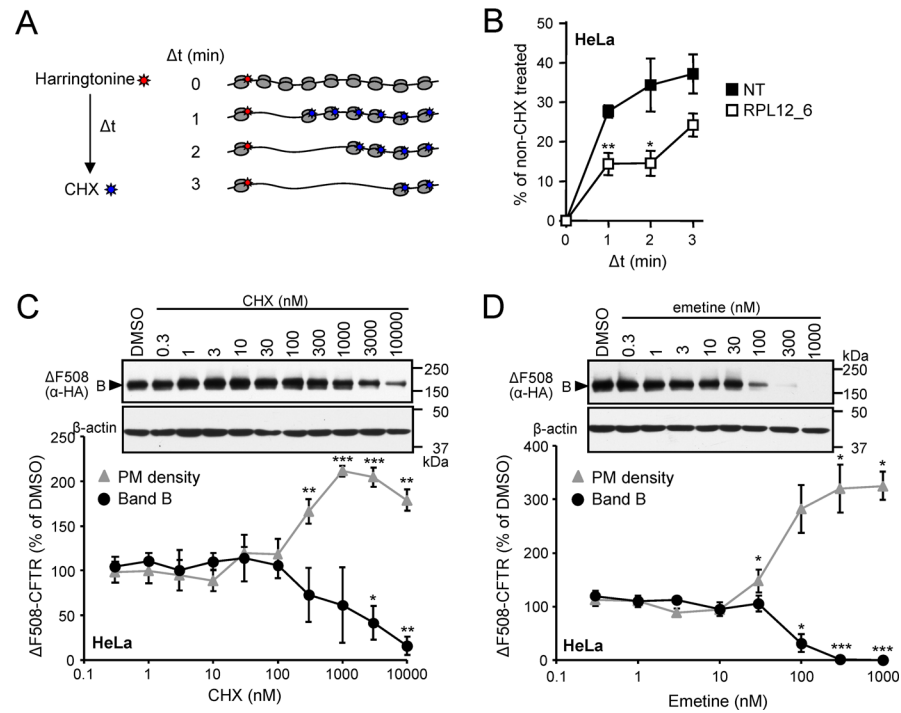


Fig 8. Slow-down of translational elongation rate partially corrects Δ F508-CFTR folding defects. (A, B) Schematic depiction of the run-off elongation experiment (A) and relative translation elongation rates in HeLa cells transfected with *RPL12* or NT siRNA (B). The values were normalized to cells in which the initiation was stopped with harringtonine (2 μ g/ml), but the run-off elongation was allowed to proceed without CHX inhibition ($n = 4$). (C, D) PM density and total expression of Δ F508-CFTR after 24 h treatment with increasing concentrations of CHX (C) or emetine (D) in HeLa. Δ F508-CFTR expression was visualized by immunoblot using anti-HA antibody, anti- β -actin antibody served as loading control (upper panels). Densitometric analysis of core-glycosylated Δ F508-CFTR expression and PM density are expressed as a percentage of DMSO controls (lower panels, $n = 3$). * $p < 0.05$; ** $p < 0.01$; *** $p < 0.001$. Error bars show SEM of 3–4 independent experiments. The underlying data of panels B–D can be found in [S1 Data](#).

doi:10.1371/journal.pbio.1002462.g008

Considering that reduced translational elongation rate following *RPL12* knockdown is associated with the reduction of the ER load, and this may influence the protein homeostasis (proteostasis) network activity [23], we measured the expression level of molecular chaperones and cochaperones, critical determinants of the proteostasis network folding capacity [11]. The expression level of HSP90A, HSPA8, AHA1, STIP1, DNAJA1, and BAG1 however, remained unaltered upon *RPL12* ablation (S8 Fig), suggesting that the ratio between the total pool of synthesized proteins and these chaperones and cochaperones was not affected by *RPL12* knockdown.

As an alternative method to test the influence of the ER load on cotranslational folding of Δ F508-CFTR, we partially inhibited translation initiation by reducing one of the core translation initiation factors, the cap-binding protein eIF4E, expression using siRNA-mediated knockdown. Reduction of the eIF4E mRNA by ~50% (S7E Fig) decreased the pulse-labeled pool of Δ F508-CFTR by ~30% (S7L Fig). This led to a 20%–30% increase in the r Δ F508-CFTR PM density and function without altering its fast PM turnover or functional stability (S7H–S7K Fig). These results are at variance with observation obtained in FRT cells upon inhibiting initiation with hippuristanol, which increased the Δ F508-CFTR activity by ~2.5-fold at the PM [72]. Thus, significant reduction of protein synthesis, including Δ F508-CFTR and the ER load by impeding translational initiation without translational elongation has a modest contribution

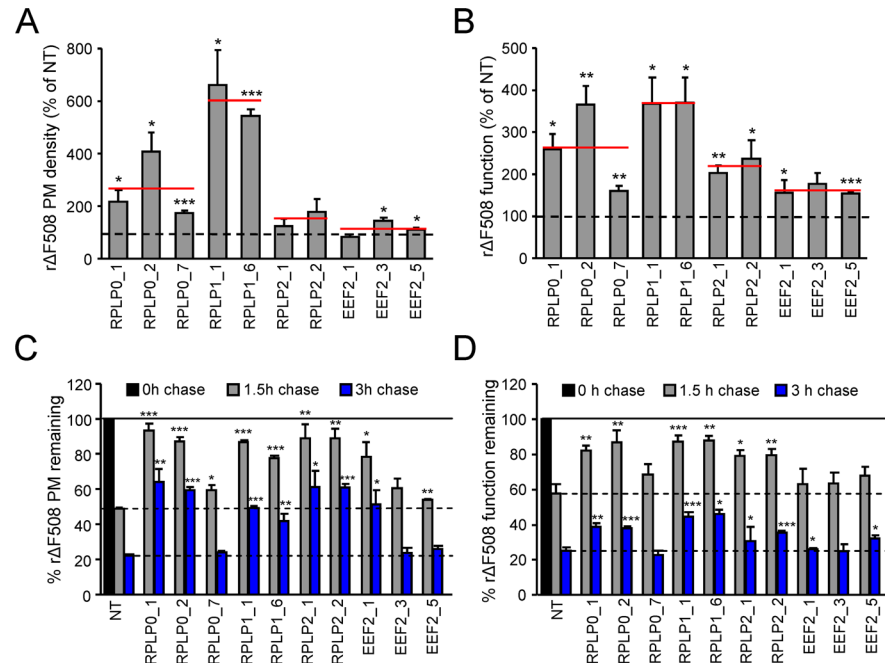


Fig 9. SiRNA-mediated silencing of ribosomal stalk proteins enhances the PM density, function, and stability of $\Delta F508$ -CFTR. (A, B) The effect of ribosomal stalk protein (RPLP0—P0, RPLP1—P1, and RPLP2—P2) and eEF-2 knockdown on the PM density (A) and function (B) of r $\Delta F508$ -CFTR in CFBE. The indicated ribosomal proteins were silenced with two to three individual siRNAs and the mean PM density or function is shown as a red line. The values are expressed as percent of NT siRNA controls ($n = 3$). (C, D) The effect of ribosomal stalk protein and eEF-2 knockdown on the PM (C, $n = 3$) and functional stability (D, $n = 3$) of r $\Delta F508$ -CFTR after 1.5 and 3 h chase at 37°C. * $p < 0.05$, ** $p < 0.01$, *** $p < 0.001$. Error bars show SEM of three independent experiments. The underlying data of panels A–D can be found in [S1 Data](#).

doi:10.1371/journal.pbio.1002462.g009

to the conformational rescue of $\Delta F508$ -CFTR, as compared to that of RPL12 silencing in CFBE and failed to provoke the accumulation of native-like, conformationally stabilized r $\Delta F508$ -CFTR at the PM.

Discussion

While technology developments significantly improved the identification of the interactome of conformationally defective polypeptides, including the $\Delta F508$ -CFTR [28–30], establishing the functional significance of interacting proteins remains a daunting task. One possible approach is offered by global, quantitative analysis of functional gene interaction in yeast models. While it is appreciated that the molecular processes involved in the translation, folding, maturation, and trafficking of integral membrane proteins are evolutionarily conserved [78], the extent to which global, quantitative analysis of gene interaction in a yeast model yields correct predictions of human genetic modifier that enhance the functional rescue of disease-causing target proteins, remains poorly understood [79,80].

Here, we show that gene interaction studies using the yeast ATP-binding cassette family C (ABCC) protein Yor1 incorporating the $\Delta F508$ -CFTR homologous mutation $\Delta F670$ can predict novel modifier genes of $\Delta F508$ -CFTR biogenesis in respiratory epithelia. Silencing six of the seven genes selected to probe various steps during Yor1- $\Delta F670$ biogenesis that acted as deletion suppressors to augment Yor1- $\Delta F670$ -dependent oligomycin resistance [39], also increased PM expression of $\Delta F508$ -CFTR in the human CFBE cells. Knockdown of *RPL12*, a component of the large ribosomal subunit stalk, increased both the ER folding efficiency as

well as the metabolic and functional stability of the mature, complex-glycosylated Δ F508-CFTR in post-ER compartments and at the PM, respectively. These results jointly indicate the conservation/concordance of gene interaction modules influencing the early biogenesis of Yor1- Δ F670 and Δ F508-CFTR, including mRNA turnover, rRNA processing, and ribosome structural assembly.

In contrast to mammalian cells, the Rpl12 protein in *S. cerevisiae* is encoded by a duplicated gene, *RPL12A* and *RPL12B*, which are remnants of a genome duplication event [81]. In the case of *RPL12* and Yor1- Δ F biogenesis, both *RPL12A* and *RPL12B* acted as deletion suppressors, but *RPL12A* knockout yielded a quantitatively greater effect. Deletion of both genes is associated with a severe growth, but not a viability defect and results in a profound decrease in the translational elongation rate, while deletion of either single gene slightly retarded cell growth and elongation [67,68].

Knockdown of Rpl12 protein expression by ~50% considerably decreased the global translational elongation rate as determined by the kinetics of run-off elongation in human CFBE cells (Fig 8B). The concomitant increase of Δ F508-CFTR PM density and function is reminiscent of a recent report by Meriin et al., demonstrating that pharmacological attenuation of translational initiation or elongation rate by hippuristanol or CHX, respectively, can partially rescue the PM functional expression defect of Δ F508-CFTR in FRT cells [72]. While the cellular and molecular mechanism of Δ F508-CFTR rescue is not known in FRT cells, here we show that *RPL12* silencing increases the ER folding efficiency of the nascent chain and the stability of both the core- and complex-glycosylated forms, as well as the PM resident Δ F508-CFTR channel. The enhanced ER folding efficiency can be attributed, at least in part, to favourable changes in the folding energetics of the mutant, as reflected by the increased thermostability of the final fold, represented by the complex-glycosylated Δ F508-CFTR in *RPL12* ablated cells (Fig 7B).

While we do not have a definitive explanation for the significantly increased co- and post-translational folding efficiency and stabilization of Δ F508-CFTR upon translational elongation slow down, similar phenomena have been demonstrated for various polypeptides in silico, in vitro as well as in vivo [62–65,82,83]. Translational rate slow down may help to reduce the amount of misfolded domain intermediates that are resistant to conformational rescue by the proteostasis machinery, influence the stability of folding intermediates of the nascent chain and/or the folding trajectory of Δ F508-CFTR by altering the binding to profolding and/or prodegradative constituents of the ribosome associated quality control machinery [84–87]. The longer residence time of the nascent chain on the ribosome may also shield against degradation and facilitate folding.

The hypothesis that reduced translation elongation increases Δ F508-CFTR folding is consistent with earlier observations showing that slowing the global translational elongation rate by various interventions can improve the folding efficiency of specific proteins in eukaryotic cells. Synonymous codon changes that result in ribosomal pausing can lead to alternate folding pathways, distinct conformations, and can facilitate cotranslational targeting of membrane proteins to the translocon [63,65,88], as has been shown for the multidrug resistance 1 gene product P-glycoprotein [62,64]. In contrast, accelerating translation rate by synonymous codon substitutions in the α -subdomain of WT-CFTR NBD1 resulted in aggregation of the full-length channel [89]. Codon optimization also resulted in conformational changes and impaired function of *Neurospora*, a clock protein [90].

The possibility that global translational attenuation by *RPL12* knockdown can exert a general profolding effect is unlikely but cannot be ruled out. *RPL12* silencing did not shift the expression levels of known CFTR modifier genes such as HSP90A, HSPA8, AHA1, STIP1, DNAJA1, and BAG1, which are molecular chaperones and cochaperones that are known modulators of Δ F508-CFTR folding and PM expression [11]. Furthermore, whereas *RPL12* siRNA

increased the PM expression of hERG-G601S and $\Delta F508$ -CFTR, and to some extent their WT-counterparts, *RPL12* ablation had no effect on the PM density of V2R-Y128S, as well as MLC1-P92S or -S280L, despite the documented recognition of these misfolded membrane proteins by the ER and PM protein quality control systems [11,55,56,58,91]. Thus, intrinsically slow and inefficient folding and domain assembly of the WT CFTR and hERG, which is further compromised by missense mutations, may sensitize these complex multidomain proteins to rescue upon translational elongation slow down.

Rpl12 is localized in the 60S subunit GAC and interacts with the GTP-bound translation factors [92–94]. Rpl12 binds to the 28S rRNA together with ribosomal protein P0 to constitute the base of the lateral ribosomal stalk (P-stalk), which serves as a binding platform for ribosomal proteins P1 and P2 [67,73,74,95,96]. The stalk is present in all eukaryotic ribosomes and plays an integral role in translation elongation, due to specific interactions of P1 and P2 with eukaryotic elongation factor 1 α (eEF-1 α) and Rpl12 with eEF-2 [92–94]. Based on evidence in yeast showing disruption of stalk components reduces translation without changing translational fidelity [68,75,76,97], we hypothesize that similar to the knockdown of *RPL12*, silencing of other ribosomal stalk proteins, which inhibits elongation factors recruitment and slows down the translational elongation, allows the development of a native-like $\Delta F508$ -CFTR conformation. Consistent with this hypothesis, silencing of P1, P2, P0, or eEF-2 increased the $\Delta F508$ -CFTR functional expression and PM stability (Fig 9).

In contrast, silencing of one of the core translation initiation factors, the cap-binding protein eIF4E, decreased $\Delta F508$ -CFTR synthesis but only slightly increased $\Delta F508$ -CFTR PM density without stabilizing the rescued mutant channel biochemically or functionally at the PM. Studies in FRT cells, however, showed that partial inhibition of translation initiation with hippuristanol leads to a substantial increased $\Delta F508$ -CFTR function [72]. Thus, the concomitant reduction of the overall ER protein load might be a contributing factor to the increased PM expression and function of $\Delta F508$ -CFTR, but is likely insufficient to explain enhanced ER folding efficiency of the mutant channel.

Our results showing that knockdown of different ribosomal stalk proteins increases the folding propensity and function of $\Delta F508$ -CFTR provide new insight into targeted slow-down of translational elongation as a possible therapeutic strategy for treating a conformational disease resulting from mutations in an evolutionarily conserved amino acid residue. Whether other ribosomal proteins and ribosome-bound soluble factors are involved in this mechanism or small molecule inhibitors can be identified to mimic the genetic effect of *RPL12* knockdown remain to be established in future work.

From a translational perspective, our findings show that *RPL12* knockdown is additive with the small-molecule corrector VX-809 in primary HBE cells with *CFTR* ^{$\Delta F508/\Delta F508$} genotype. Moreover, the treatment combination restores $\Delta F508$ -CFTR function to ~50% of the WT level, a value that is deemed sufficient to alleviate CF clinical manifestations, since heterozygous carriers do not show disease symptoms [98]. Knockdown of other ribosomal stalk proteins and the translational elongation factor eEF-2, similarly result in improved $\Delta F508$ -CFTR biogenesis. Thus, ribosomal stalk perturbation represents a potential target for rescuing the $\Delta F508$ -CFTR biogenesis in combination with VX-809, which represents one of the most efficacious strategies for the correction of $\Delta F508$ -CFTR thus far [20]. Future work will clarify the mechanism by which the reduced translational elongation rate via reduced function of the ribosomal stalk could be used to treat ~90% of CF patients afflicted with this most common allele. Furthermore, application of yeast phenomics as part of an integrative research approach should be considered for its potential to discover genotype-phenotype networks that can guide discovery of new therapeutics for patients with CF and possibly other diseases that can be modeled in *S. cerevisiae*.

Materials and Methods

Ethics Statement

Human lung tissues were obtained from $CFTR^{WT/WT}$ non-CF and $CFTR^{\Delta F508/\Delta F508}$ CF individuals under the protocol and consent form approved by the Institutional Review Board at University of Alabama Birmingham (IRB #X080625002). All adult participants provided informed consent, or a parent or guardian of any child participant provided informed permission on their behalf. All consent was obtained in written form.

Reagents and Antibodies

SiRNA was purchased from Qiagen, dsiRNA were obtained from Integrated DNA Technologies, and the target sequences are listed in [S1 Table](#). The following antibodies were used: monoclonal mouse anti-HA (MMS101R, Covance), monoclonal mouse anti-CFTR antibodies (10B6.2, 570 and 596, Cystic Fibrosis Foundation Therapeutics, Inc.), polyclonal rabbit anti-Rpl12 (AP16275c, Abgent), polyclonal rabbit anti-Rpl12 (ab157130, abcam), monoclonal rat anti-HSP90A (9D2, Enzo), monoclonal rat anti-HSPA8 (1B5, Enzo), mouse monoclonal anti-HSPA4 (C92F3A-5, Enzo), monoclonal mouse anti-AHA1 (1A2-A8, Abnova), monoclonal mouse anti-STIP1 (DS14F5, Enzo), polyclonal rabbit anti-DNAJA1 (ADI-SPA-405, Enzo), monoclonal mouse anti-BAG1 (4A2, Enzo), monoclonal mouse anti-Mucin5A/C (45M1, ThermoScientific), monoclonal mouse anti-acetylated tubulin (6-11B-1, Sigma), polyclonal rabbit anti-occludin (Zymed), monoclonal mouse anti- Na^+/K^+ -ATPase (H3, Santa Cruz Biotechnology), monoclonal mouse anti- β actin (ab8226, abcam), and monoclonal mouse anti- β actin (AC-15, Sigma). The TfR PM density was detected using HRP-conjugated transferrin (090-030-050, Jackson ImmunoResearch), and actin was labeled for immunofluorescence microscopy using A555 conjugated Acti-stain (Cytoskeleton).

Yeast Strains and Media

Yeast deletion mutant strains were obtained from Research Genetics. To retest selected hits, four single-colony deletion mutant clones were selected for construction of double mutants by the SGA, as described [44,45]. The query allele of the RL8 strain (described in [39]) was modified by substitution for the *Tet* promoter with the *ACT1* promoter (*Pact1*) and without the C-terminal GFP tag to obtain the *Pact1-yor1-F670-R1116T-HA* allele. To construct this allele, the pJ023 plasmid was modified by replacing the tetracycline promoter element with 680 bp of the 5' UTR of *ACT1* promoter and then used to construct *Pact1-yor1- $\Delta F670$ -R1116T-HA* (the R1116T second site mutation is described in [36]) by integrating it at the *YOR1* promoter of LMY789, containing the *yor1- $\Delta F670$ -R1116T-HA* allele (gift from Elizabeth Miller). After SGA, frozen glycerol stocks were made for subsequent Q-HTCP analysis. YPEG media was made with 10 g/L yeast extract, 20 g/L peptone, 3% ethanol, and 3% glycerol.

Q-HTCP

Q-HTCP was performed as previously described [46], assessing gene interaction by comparison of the cell proliferation parameter, L (the time (hours) after which half carrying capacity is reached), obtained from growth curves for single and double mutant cultures across a range of perturbation intensity using different growth-inhibitory concentrations of oligomycin, the primary substrate of Yor1. Hundreds of replicates of the single mutant, Yor1- $\Delta F670$, were used to obtain the range of L at each condition tested. Interaction was calculated as the difference between the L values for the double mutant and the Yor1- $\Delta F670$ single mutant, after

normalizing all data by the difference in L between the double mutant and the Yor1- $\Delta F670$ single mutant reference median in media not containing oligomycin, as previously described [39].

Cell Culture and Media

Human lung tissues were obtained from $CFTR^{WT/WT}$ non-CF and $CFTR^{\Delta F508/\Delta F508}$ CF individuals (patient code 21, 22, and 48) under the protocol and consent form approved by the Institutional Review Board at University of Alabama Birmingham (IRB #X080625002). Cell isolation was performed as described [51,99]. After expansion, first or second passage cells were transferred to permeable filter supports and allowed to differentiate under air-liquid interface conditions for 3 wk as described in [100,101]. Alternatively, HBE cells (patient code BCFr43 and BCF121209) were purchased from the Cystic Fibrosis Translational Research center (CFTRc) at McGill University, expanded following the conditional reprogramming protocol described in [102] followed by differentiation on permeable filter supports under air-liquid interface using the Vertex conditions [100].

The generation and maintenance of the CFBE cell lines, expressing WT- or $\Delta F508$ -CFTR with a 3HA-tag in the 4th extracellular loop under the control of a tetracycline-inducible transactivator was described before [17,48]. Generation of stable CFBE cell lines constitutively expressing WT- or $\Delta F508$ -CFTR has been described and these cell lines are depicted as CFBE^C [51,52] to distinguish them from the inducible CFBE expression system. The HeLa cells constitutively expressing extracellular 3HA-tagged WT- or $\Delta F508$ -CFTR have been described previously [11].

SiRNA Transfection

In CFBE cells, the target genes were silenced by forward transfection using 50 nM siRNA (Qiagen) and Lipofectamine RNAiMAX (Invitrogen). Transfected cells were allowed to polarize for 5 d. For studies in filter grown CFBE cells, 100 nM siRNA duplexes were introduced by reverse transfection using an established protocol [53]. HeLa cells were transfected using Oligofectamine (Invitrogen) as described previously [11], and the experiments were performed 4 d after transfection. HBE cells were either reverse transfected with dsRNA (Integrated DNA Technologies) using Lipofectamine RNAiMAX [53] or were forward transfected for 6 h 1 d postseeding with 50 nM NT or RPL12_6 siRNA and the transfections were repeated every 7 d. Monolayers were cultured for a total of 21 d.

PM Density Measurement

PM densities of extracellular HA-tagged proteins were determined by cell surface ELISA [11]. The TfR PM density was measured by the specific binding of HRP-conjugated transferrin. The relative amount of transferrin-HRP or HRP-conjugated secondary antibodies was measured by luminescence, using a VICTOR Light plate reader (PerkinElmer) after addition of 50 μ l/well HRP-Substrate (SuperSignal West Pico, Thermo Fisher Scientific). PM density measurements were normalized for cell number, determined by Alamar Blue assay (Invitrogen) or protein concentration, determined by bicinchoninic acid assay (BCA, Pierce).

CFTR or TMEM16A Conductance Measurement by Halide-Sensitive YFP Quenching Assay

The halide-sensitive YFP quenching assay has been used before to determine the PM function of CFTR [19] or TMEM16A [48]. Briefly, $\Delta F508$ -CFTR was activated by well-wise injection of 50 μ l/well activator solution (20 μ M Frk, 0.5 mM IBMX, 0.5 mM cpt-cAMP and 100 μ M gen in

PBS) followed by 100 μ l PBS-iodide in which NaCl was replaced with NaI after a delay of 60 s. TMEM16A was activated by well-wise injection of 50 μ l/well 100 μ M ATP in PBS followed by 100 μ l PBS-iodide after a delay of 6 s.

Immunoblotting

For immunoblot analysis, cells were lysed either with NP-40-based lysis buffer (150 mM NaCl, 1% NP-40, 50 mM Tris-HCl, pH 8.0) or RIPA (ThermoScientific) in the presence of Halt protease inhibitor cocktail (ThermoScientific). Following total protein quantification using the BCA assay (ThermoScientific), equal amounts of protein were mixed with 4X loading buffer, incubated at 37°C for 10 min, resolved by SDS-PAGE, and blotted onto PVDF membranes. Following antibody binding, signals were detected using the SuperSignal West Femto (ThermoScientific) or Luminata Crescendo (EMD Millipore) substrates and quantified on a ChemiDocXRS (Bio-Rad) or by densitometry using ImageJ.

Thermoaggregation Assay

Thermoaggregation assays were performed as previously described [66]. Briefly, following cell lysis with RIPA buffer, the lysates were cleared by centrifugation and the aggregation tendency of WT- and Δ F508-CFTR was compared after exposing the lysates to 20–80°C for 15 min. Macromolecular aggregates were eliminated by centrifugation (15,000 \times g for 15 min). The remaining soluble WT- and Δ F508-CFTR, and HSPA4 in the supernatant was measured by quantitative immunoblotting.

I_{sc} Measurement

CFBE or HBE cells expressing WT- or Δ F508-CFTR were grown to confluence on permeable filters at an air-liquid interface and mounted in modified Ussing chambers. I_{sc} measurements were obtained under voltage clamp conditions using MC8 equipment and P2300 Ussing chambers (Physiologic Instruments) as previously described [51,52,103]. Cells were equilibrated for 5–10 min in regular Ringer solution (115 mM NaCl, 25 mM NaHCO₃, 2.4 mM KH₂PO₄, 1.24 mM K₂HPO₄, 1.2 mM CaCl₂, 1.2 mM MgCl₂, 10 mM D-glucose, pH 7.4). In some measurements, this was followed by the exchange of low chloride Ringer (115 mM NaCl reduced to 1.2 mM NaCl and 10 mM D-glucose replaced with 115 mM Na-gluconate) to the apical surface. After addition of the sodium channel inhibitor amiloride (100 μ M), the CFTR agonists Frk (10 μ M) and gen (50 μ M) were sequentially added, followed by inhibitor₁₇₂ (10 μ M) at the conclusion of each experiment, in order to specifically inhibit CFTR activity. Changes in CFTR-mediated ion transport were calculated using the highest current value for each sample after achievement of a stable plateau for several minutes.

Metabolic Pulse-Chase Studies

Experiments were performed essentially as described [104]. Briefly, 4–5 d after NT or *RPL12* siRNA transfection, CFBE (or HeLa) cells expressing Δ F508-CFTR were pulse-labeled with 0.2 mCi/ml (or 0.1 mCi/ml for HeLa cells) ³⁵S-methionine and ³⁵S-cysteine (EasyTag Express Protein Labeling Mix, PerkinElmer) in cysteine and methionine-free medium for 30 min for CFBE (or 20 min for HeLa) at 26°C or 37°C (incorporation efficiency) or labeled for 3 h at 26°C and then chased 2 h at 37°C in full medium (maturation efficiency). Radioactivity incorporated into the core- and complex-glycosylated glycoproteins was visualized by fluorography and quantified by phosphoimage analysis using a Typhoon imaging platform (GE Healthcare). For depiction of representative images, autoradiographs were acquired by film-exposure.

For the experiments involving VX-809, NT, or *RPL12*, siRNA-transfected HeLa cells expressing Δ F508-CFTR were treated with 3 μ M VX-809 or DMSO for 24 h before the experiment. Cells were pulse-labeled with 0.1 mCi/ml for 20 min and chased 2 h at 37°C in the presence or absence of VX-809. The maturation efficiency was determined by calculating the percent of pulse-labeled immature, core-glycosylated Δ F508-CFTR conversion into the mature, complex-glycosylated form. To allow for the detection of the low percentage of complex-glycosylated Δ F508-CFTR, the total labeling for 3 h was extrapolated from values obtained for 20 or 30 min pulse labeled samples.

Ribosomal Run-Off Assay

HeLa cell transfected with either NT or *RPL12_6* siRNA were treated with harringtonine (2 μ g/ml) to stop translation initiation [69]. Ongoing elongation was quantified by the metabolic pulse chase technique, using 35 S-methionine and 35 S-cysteine. The run-off elongation was terminated after 1–3 min with CHX (100 μ g/ml). The cell lysates were separated by SDS-PAGE and the total radioactive signal of fluorographs was measured by phosphoimage analysis. The signals were normalized for the amount of protein loaded and expressed as percentage on non-CHX-treated controls.

Q-PCR

Q-PCR was performed as described previously [48]. The primers are listed in [S2 Table](#).

Immunostaining and Fluorescence Microscopy

Filter-grown differentiated HBE cells were washed with PBS containing 5 mM DL-dithiothreitol for 5 min on ice to remove mucin. Cells were fixed in 4% paraformaldehyde and permeabilized with 0.2% Triton X-100. For occludin staining, cells were pre-extracted with 0.2% Triton X-100 for 2 min before fixation. After blocking in PBSCM (PBS containing 1 mM MgCl₂, 0.1 mM CaCl₂) with 0.5% bovine serum albumin, cells were incubated with primary antibodies overnight at 4°C, washed with PBSCM, and stained with Alexa-Fluor-conjugated secondary antibodies (1:1000) or Acti-stain (1:300) for 1 h at room temperature. Nuclei were stained with DAPI. Cut-out pieces of filter were mounted on glass slides, and optical stacks were acquired using a laser confocal fluorescence microscope (LSM780 Carl Zeiss) equipped with a 63X/1.40 oil DICIII Plan apochromat objective. Typically 20–30 optical xy-sections were acquired and reconstituted using the Zen 2012 software, and representative xz-sections are shown.

Statistical Analysis

Results are presented as mean \pm SEM with the number of experiments indicated. Statistical analysis was performed by two-tailed Student's *t* test with the means of at least three independent experiments, and the 95% confidence interval was considered significant.

Supporting Information

S1 Data. Numerical values used in preparation of Figs [1A–1E](#), [2A](#), [2C](#), [2E](#), [2F](#), [3A–3E](#), [4A–4C](#), [5B–5D](#), [6A–6F](#), [7B](#), [7D–7H](#), [8B–8D](#), [9A–9D](#), [S1B](#), [S2C–S2E](#), [S3B–S3E](#), [S4C](#), [S5A–S5C](#), [S5E](#), [S5F](#), [S6A–S6C](#), [S7A–S7E](#) and [S7H–S7L](#).

(XLS)

S1 Fig. Analysis of hits from genome-wide screen for modifiers of Yor1- Δ F670 biogenesis.

(A) The top 180 deletion suppressors [39] were reanalyzed using the DAVID bioinformatics tool and functional annotation clustering. Two clusters were identified with an enrichment

score of 5.68 (left panel) and 4.78 (right panel). Only genes with more than three associations to gene ontology (GO) terms, SwissProt—Protein Information Resource (SP_PIR) keywords or Kyoto Encyclopedia of Genes and Genomes (KEGG) pathways are shown. Genes selected for further study are highlighted in red. **(B)** Scatter plot of the change in the cell proliferation parameter L (ΔL) for 0.25 $\mu\text{g/ml}$ oligomycin in *yor1*- $\Delta F670$. Oligomycin resistance was compared between the single mutant (control) and the indicated double mutant cultures. The same results depicted as box-whisker plots are shown in [Fig 1B–1E](#). ** $p < 0.01$; *** $p < 0.001$. The underlying data of panel B can be found in [S1 Data](#).

(TIF)

S2 Fig. Halide-sensitive YFP quenching assay in CFBE cells expressing $\Delta F508$ -CFTR. **(A, B)** Representative traces of r $\Delta F508$ -CFTR function assayed by halide-sensitive YFP quenching in CFBE cells in combination with knockdown with two individual siRNAs per indicated gene after 0 h (A) or 3 h (B) chase at 37°C. CFBE cells expressing inducible $\Delta F508$ -CFTR and constitutive halide-sensitive YFP-F46L/H148Q/I152L were transfected with siRNA. The $\Delta F508$ -CFTR function was measured by determining the YFP quenching kinetics in response to extracellular iodide addition in the presence of Frk (10 μM), IBMX (250 μM), cpt-cAMP (250 μM) and gen (50 μM). **(C)** Correlation between the r $\Delta F508$ -CFTR function as depicted in [Fig 2C](#) and the TMEM16A function monitored by iodide-mediated YFP quenching in CFBE in combination with knockdown of the *Yor1*- $\Delta F670$ modifier homologs ($n = 2$). **(D)** Correlation between the r $\Delta F508$ -CFTR PM density as depicted in [Fig 2A](#) and TfR PM density determined by transferrin-HRP binding ($n = 3$). **(E)** Correlation between the r $\Delta F508$ -CFTR PM density as depicted in [Fig 2A](#) and MLC1-S280L PM density determined by cell surface ELISA ($n = 3$). Error bars indicate SEM of 2–6 independent experiments. The underlying data of panels C–E can be found in [S1 Data](#).

(TIF)

S3 Fig. The effect of siRNA-mediated *RPL12* knockdown on the PM density and function of $\Delta F508$ -CFTR. **(A, B)** Knockdown efficiency of *RPL12* by two individual siRNAs was determined in polarized CFBE after 5 days of transfection by immunoblotting (A) or qPCR (B, $n = 3$). **(C)** Effect of *RPL12* knockdown on the PM density of r $\Delta F508$ -CFTR in HeLa cells ($n = 5$). **(D, E)** Representative I_{sc} recordings (upper panel) and quantification of the changes (ΔI_{sc} , lower panel) after siRNA-mediated *RPL12* knockdown, NT siRNA or mock transfection in CFBE cell monolayers expressing WT CFTR (D, $n = 5$), or HBE cells homozygous for WT CFTR from one donor (E, $n = 3$, donor code 10). CFTR-mediated currents were induced by sequential addition of Frk (10 μM) and gen (50 μM) followed by CFTR inhibition with inhibitor₁₇₂ (10 μM) in the presence of a basolateral-to-apical chloride gradient. ** $p < 0.01$; *** $p < 0.001$. Error bars indicate SEM of 3–5 independent experiments. The underlying data of panels B–E can be found in [S1 Data](#).

(TIF)

S4 Fig. *RPL12* silencing in HBE, alone or in combination with VX-809, increases the $\Delta F508$ -CFTR function but does not affect differentiation or morphology of the cells. **(A)** Knockdown efficiency of *RPL12* by two individual dsRNAs in polarized HBE 21 d after transfection determined by immunoblot. **(B, C)** Representative I_{sc} recordings (B) and quantification of the changes in I_{sc} upon CFTR inhibition with Inh₁₇₂ (ΔI_{sc} Inh₁₇₂, C) after dsRNA-mediated *RPL12* knockdown or NT dsRNA transfection in HBE cells homozygous for $\Delta F508$ -CFTR CFTR (patient codes BCFr34 and BCF121209, $n = 3$). CFTR mediated currents were induced by sequential addition of Frk (20 μM) and gen (50 μM) followed by CFTR inhibition with Inh₁₇₂ (20 μM) in the presence of equimolar chloride concentrations in both chambers. **(D, E)**

Characterization of HBE cells in the presence of *RPL12* silencing. Primary HBE from two patients with *CFTR* ^{$\Delta F508/\Delta F508$} genotype (D-BCFr43, E-BCF121209) were transfected with control (NT) or *RPL12* (RPL12_6 and _12) dsRNAs and differentiated for 3 wk at air-liquid interface. The cells were fixed, permeabilized, and differentiation of the pseudostratified epithelial layer was verified by the presence of ciliated cells (acetylated tubulin, Ac.tub.), goblet cells (mucin5A/C) and the staining pattern of occluding, a tight-junctions marker. DAPI was used to stain nuclei. Dotted lines show the filter, Ap, apical, scale bar = 10 μ m. The transepithelial resistance, an indirect marker of the integrity of the monolayer was also preserved (NT 403: \pm 50 Ω /cm², RPL12_6: 351 \pm 27 Ω /cm², RPL12_11: 384 \pm 45 Ω /cm²). Error bars show SEM of three independent experiments. The underlying data of panel C can be found in [S1 Data](#). (TIF)

S5 Fig. *RPL12* silencing does not increase $\Delta F508$ -CFTR mRNA expression, but augments the fractional Frk stimulated current. (A) Relative amount of CFTR mRNA in CFBE cells upon transfection with *RPL12* or NT siRNAs determined by qPCR ($n = 3$). (B) Cell number determined by Alamar blue assay ($n = 3$) or protein concentration measured by BCA assay ($n = 3$) of CFBE upon *RPL12* knockdown for 5 d in comparison to NT siRNA or 24 h treatment with VX-809 (3 μ M). (C) Determination of [³⁵S]-methionine/cysteine incorporation during the labeling period into the nascent $\Delta F508$ -CFTR (pulse 10 min) at 37°C in *RPL12* or NT siRNA treated HeLa cells ($n = 3$). (D) Following *RPL12* knockdown at 37°C in CFBE^C cells, the half-life of $\Delta F508$ -CFTR was determined by immunoblot with CHX chase. Visualization of CFTR was achieved using 10B6.2 antibody, and anti- β -actin antibody was utilized as a loading control. (E, F) Fractional Frk-stimulated activity of $\Delta F508$ -CFTR in CFBE^C (E, $n = 5$) or HBE (F, $n = 4$) with *CFTR* ^{$\Delta F508/\Delta F508$} genotype. The relative Frk sensitivity was calculated as a ratio of I_{sc} stimulated with Frk (10 μ M) over Frk and gen (50 μ M) as shown in Figs [3E](#) and [4B](#). * $p < 0.05$, ** $p < 0.01$; *** $p < 0.001$. Error bars show SEM of 3–5 independent experiments. The underlying data of panels A–C, E, and F can be found in [S1 Data](#). (TIF)

S6 Fig. *RPL12* silencing effect on the stability of misfolded PM proteins in HeLa cells. (A–C) PM stability determined by cell surface ELISA in NT or *RPL12* siRNA treated HeLa cells. Cells stably expressing extracellular HA-epitope tagged V2R-Y128S (A, $n = 3$), MLC1-P92S or -S280L (B, $n = 3$), or hERG-WT or -G601S (C, $n = 4$) were used. SiRNAs for CHIP and Tsg101 served as positive controls that attenuated the peripheral removal of misfolded membrane proteins. The amount remaining after initial labeling is calculated as percent after the indicated chase time. * $p < 0.05$; ** $p < 0.01$; *** $p < 0.001$. Error bars are SEM of 3–4 independent experiments. The underlying data of panels A–C can be found in [S1 Data](#). (TIF)

S7 Fig. Ribosomal stalk protein, eEF-2 and eIF4E knockdown in CFBE cells. (A–E) Knockdown efficiency of RPLP0 (A), RPLP1 (B), RPLP2 (C), eEF-2 (D), and eIF4E (E) in polarized CFBE 5 d after transfection as determined by qPCR ($n = 3$). (F, G) Correlation between the knockdown efficiency of RPLP0, RPLP1, RPLP2 or eEF-2 and the r $\Delta F508$ -CFTR PM density (F) or function (G). (H, J) The effect of the core initiation factor eIF4E knockdown on the PM density (H) and function (J) of r $\Delta F508$ -CFTR in CFBE. The values are expressed as percent of NT siRNA controls ($n = 3$). (I, K) The effect of eIF4E silencing on the PM (I, $n = 3$) and functional stability (K, $n = 3$) of r $\Delta F508$ -CFTR after 1.5 and 3 h chase at 37°C. (L) [³⁵S]-methionine and [³⁵S]-cysteine incorporation during the labeling period (15 min) at 37°C into the newly formed $\Delta F508$ -CFTR in CFBE cells transfected with EIF4E or NT siRNA ($n = 4$). * $p < 0.05$; ** $p < 0.01$; *** $p < 0.001$. Error bars show SEM of 3–6 independent experiments. The

underlying data of panels A–E and H–L can be found in [S1 Data](#).
(TIF)

S8 Fig. The effect of *RPL12* knockdown on CFTR-associated chaperones. Expression of the CFTR-associated chaperones and cochaperones HSP90A, HSPA8, Aha1, STIP1, DNAJA1 and BAG1 was determined by immunoblot analysis upon knockdown of *RPL12*. β -actin and Na^+/K^+ -ATPase served as loading controls.
(TIF)

S1 Table. SiRNAs used in this study.
(PDF)

S2 Table. Q-PCR primers used in this study.
(PDF)

Acknowledgments

We thank Dr. D. Gruenert (University of California, San Francisco) for the parental CFBE41o-cell line. Dr. Jeong Hong (Gregory Fleming James Cystic Fibrosis Research Center, Birmingham, AL) for assistance with CFBE41o- culture and immunoblotting, Hui Wen (Gregory Fleming James Cystic Fibrosis Research Center, Birmingham, AL) for assistance with short circuit current measurement techniques, Marina Mazur (Gregory Fleming James Cystic Fibrosis Research Center, Birmingham, AL) for the primary HBE cultures, and John Rodgers (University of Alabama at Birmingham) and Rick White (University of British Columbia) for assistance with yeast phenomic analysis.

Author Contributions

Conceived and designed the experiments: GV KO PMA JLH GLL. Performed the experiments: GV KO PMA DP ABM STL JG MI. Analyzed the data: GV KO PMA DP ABM JG MI JLH. Wrote the paper: GV KO EJS JLH GLL.

References

1. Trezise AE, Buchwald M. In vivo cell-specific expression of the cystic fibrosis transmembrane conductance regulator. *Nature*. 1991; 353(6343):434–7. Epub 1991/10/03. doi: [10.1038/353434a0](#) PMID: [1716739](#).
2. Collins FS. Cystic fibrosis: molecular biology and therapeutic implications. *Science*. 1992; 256(5058):774–9. Epub 1992/05/08. PMID: [1375392](#).
3. Sosnay PR, Siklosi KR, Van Goor F, Kaniecki K, Yu H, Sharma N, et al. Defining the disease liability of variants in the cystic fibrosis transmembrane conductance regulator gene. *Nat Genet*. 2013; 45(10):1160–7. Epub 2013/08/27. ng.2745 [pii] doi: [10.1038/ng.2745](#) PMID: [23974870](#).
4. Cystic Fibrosis Mutation Database. Available: <http://www.genet.sickkids.on.ca/app>.
5. Veit G, Avramescu RG, Chiang AN, Houck SA, Cai Z, Peters KW, et al. From CFTR biology toward combinatorial pharmacotherapy: expanded classification of cystic fibrosis mutations. *Mol Biol Cell*. 2016; 27(3):424–33. Epub 2016/01/30. 27/3/424 [pii] doi: [10.1091/mbc.E14-04-0935](#) PMID: [26823392](#); PubMed Central PMCID: PMC4751594.
6. Riordan JR, Rommens JM, Kerem B, Alon N, Rozmahel R, Grzelczak Z, et al. Identification of the cystic fibrosis gene: cloning and characterization of complementary DNA. *Science*. 1989; 245(4922):1066–73. Epub 1989/09/08. PMID: [2475911](#).
7. Cheng SH, Gregory RJ, Marshall J, Paul S, Souza DW, White GA, et al. Defective intracellular transport and processing of CFTR is the molecular basis of most cystic fibrosis. *Cell*. 1990; 63(4):827–34. Epub 1990/11/16. 0092-8674(90)90148-8 [pii]. PMID: [1699669](#).
8. Lukacs GL, Mohamed A, Kartner N, Chang XB, Riordan JR, Grinstein S. Conformational maturation of CFTR but not its mutant counterpart (Δ F508) occurs in the endoplasmic reticulum and requires

- ATP. *EMBO J.* 1994; 13(24):6076–86. Epub 1994/12/15. PMID: [7529176](#); PubMed Central PMCID: PMC395586.
9. Du K, Sharma M, Lukacs GL. The DeltaF508 cystic fibrosis mutation impairs domain-domain interactions and arrests post-translational folding of CFTR. *Nat Struct Mol Biol.* 2005; 12(1):17–25. PMID: [15619635](#).
 10. Lukacs GL, Chang XB, Bear C, Kartner N, Mohamed A, Riordan JR, et al. The delta F508 mutation decreases the stability of cystic fibrosis transmembrane conductance regulator in the plasma membrane. Determination of functional half-lives on transfected cells. *J Biol Chem.* 1993; 268(29):21592–8. Epub 1993/10/15. PMID: [7691813](#).
 11. Okiyoneda T, Barriere H, Bagdany M, Rabeh WM, Du K, Hohfeld J, et al. Peripheral protein quality control removes unfolded CFTR from the plasma membrane. *Science.* 2010; 329(5993):805–10. PMID: [20595578](#). doi: [10.1126/science.1191542](#)
 12. Hanrahan JW, Sampson HM, Thomas DY. Novel pharmacological strategies to treat cystic fibrosis. *Trends Pharmacol Sci.* 2013; 34(2):119–25. Epub 2013/02/06. S0165-6147(12)00198-8 [pii] doi: [10.1016/j.tips.2012.11.006](#) PMID: [23380248](#).
 13. Amin R, Ratjen F. Emerging drugs for cystic fibrosis. *Expert Opin Emerg Drugs.* 2014. Epub 2014/02/01. doi: [10.1517/14728214.2014.882316](#) PMID: [24479826](#).
 14. Rowe SM, Verkman AS. Cystic fibrosis transmembrane regulator correctors and potentiators. *Cold Spring Harb Perspect Med.* 2013; 3(7). Epub 2013/07/03. 3/7/a009761 [pii] doi: [10.1101/cshperspect.a009761](#) PMID: [23818513](#).
 15. Eckford PD, Ramjeeasingh M, Molinski S, Pasyk S, Dekkers JF, Li C, et al. VX-809 and related corrector compounds exhibit secondary activity stabilizing active F508del-CFTR after its partial rescue to the cell surface. *Chem Biol.* 2014; 21(5):666–78. Epub 2014/04/15. S1074-5521(14)00108-2 [pii] doi: [10.1016/j.chembiol.2014.02.021](#) PMID: [24726831](#).
 16. Loo TW, Bartlett MC, Clarke DM. Corrector VX-809 stabilizes the first transmembrane domain of CFTR. *Biochem Pharmacol.* 2013; 86(5):612–9. Epub 2013/07/10. S0006-2952(13)00415-2 [pii] doi: [10.1016/j.bcp.2013.06.028](#) PMID: [23835419](#).
 17. Okiyoneda T, Veit G, Dekkers JF, Bagdany M, Soya N, Xu H, et al. Mechanism-based corrector combination restores DeltaF508-CFTR folding and function. *Nat Chem Biol.* 2013; 9(7):444–54. Epub 2013/05/15. nchembio.1253 [pii] doi: [10.1038/nchembio.1253](#) PMID: [23666117](#).
 18. Ren HY, Grove DE, De La Rosa O, Houck SA, Sopha P, Van Goor F, et al. VX-809 corrects folding defects in cystic fibrosis transmembrane conductance regulator protein through action on membrane-spanning domain 1. *Mol Biol Cell.* 2013; 24(19):3016–24. Epub 2013/08/09. mbc.E13-05-0240 [pii] doi: [10.1091/mbc.E13-05-0240](#) PMID: [23924900](#); PubMed Central PMCID: PMC3784376.
 19. Veit G, Avramescu RG, Perdomo D, Phuan PW, Bagdany M, Apaja PM, et al. Some gating potentiators, including VX-770, diminish Δ F508-CFTR functional expression. *Sci Transl Med.* 2014; 6(246):246ra97. Epub 2014/08/08. 6/246/246ra97 [pii] doi: [10.1126/scitranslmed.3008889](#) PMID: [25101887](#).
 20. Wainwright CE, Elborn JS, Ramsey BW, Marigowda G, Huang X, Cipolli M, et al. Lumacaftor-ivacaftor in Patients with Cystic Fibrosis Homozygous for Phe508del CFTR. *N Engl J Med.* 2015; 373(3):220–31. Epub 2015/05/20. doi: [10.1056/NEJMoa1409547](#) PMID: [25981758](#); PubMed Central PMCID: PMC4764353.
 21. Veit G, Avramescu RG, Perdomo D, Phuan PW, Bagdany M, Apaja PM, et al. Some gating potentiators, including VX-770, diminish DeltaF508-CFTR functional expression. *Sci Transl Med.* 2014; 6(246):246ra97. Epub 2014/08/08. 6/246/246ra97 [pii] doi: [10.1126/scitranslmed.3008889](#) PMID: [25101887](#).
 22. Cholon DM, Quinney NL, Fulcher ML, Esther CR Jr., Das J, Dokholyan NV, et al. Potentiator ivacaftor abrogates pharmacological correction of DeltaF508 CFTR in cystic fibrosis. *Sci Transl Med.* 2014; 6(246):246ra96. Epub 2014/08/08. 6/246/246ra96 [pii] doi: [10.1126/scitranslmed.3008680](#) PMID: [25101886](#).
 23. Balch WE, Roth DM, Hutt DM. Emergent properties of proteostasis in managing cystic fibrosis. *Cold Spring Harb Perspect Biol.* 2011; 3(2). Epub 2011/03/23. cshperspect.a004499 [pii] doi: [10.1101/cshperspect.a004499](#) PMID: [21421917](#); PubMed Central PMCID: PMC3039536.
 24. Collawn JF, Fu L, Bebok Z. Targets for cystic fibrosis therapy: proteomic analysis and correction of mutant cystic fibrosis transmembrane conductance regulator. *Expert Rev Proteomics.* 2010; 7(4):495–506. Epub 2010/07/27. doi: [10.1586/epr.10.45](#) PMID: [20653506](#); PubMed Central PMCID: PMC2927865.
 25. Stefano DD, Villella VR, Esposito S, Tosco A, Sepe A, Gregorio FD, et al. Restoration of CFTR function in patients with cystic fibrosis carrying the F508del-CFTR mutation. *Autophagy.* 2014; 10(11):2053–74. Epub 2014/10/29. 973737 [pii] doi: [10.4161/15548627.2014.973737](#) PMID: [25350163](#).

26. Corvol H, Blackman SM, Boelle PY, Gallins PJ, Pace RG, Stonebraker JR, et al. Genome-wide association meta-analysis identifies five modifier loci of lung disease severity in cystic fibrosis. *Nat Commun*. 2015; 6:8382. Epub 2015/09/30. ncomms9382 [pii] doi: [10.1038/ncomms9382](https://doi.org/10.1038/ncomms9382) PMID: [26417704](https://pubmed.ncbi.nlm.nih.gov/26417704/); PubMed Central PMCID: PMC4589222.
27. Gallati S. Disease-modifying genes and monogenic disorders: experience in cystic fibrosis. *Appl Clin Genet*. 2014; 7:133–46. Epub 2014/07/24. doi: [10.2147/TACG.S18675tacc-7-133](https://doi.org/10.2147/TACG.S18675tacc-7-133) [pii]. PMID: [25053892](https://pubmed.ncbi.nlm.nih.gov/25053892/); PubMed Central PMCID: PMC4104546.
28. Wang X, Venable J, LaPointe P, Hutt DM, Koulou AV, Coppinger J, et al. Hsp90 cochaperone Aha1 downregulation rescues misfolding of CFTR in cystic fibrosis. *Cell*. 2006; 127(4):803–15. Epub 2006/11/18. S0092-8674(06)01378-X [pii] doi: [10.1016/j.cell.2006.09.043](https://doi.org/10.1016/j.cell.2006.09.043) PMID: [17110338](https://pubmed.ncbi.nlm.nih.gov/17110338/).
29. Rauniyar N, Gupta V, Balch WE, Yates JR, 3rd. Quantitative proteomic profiling reveals differentially regulated proteins in cystic fibrosis cells. *J Proteome Res*. 2014; 13(11):4668–75. Epub 2014/05/14. doi: [10.1021/pr500370g](https://doi.org/10.1021/pr500370g) PMID: [24818864](https://pubmed.ncbi.nlm.nih.gov/24818864/); PubMed Central PMCID: PMC4224989.
30. Pankow S, Bamberger C, Calzolari D, Martinez-Bartolome S, Lavalley-Adam M, Balch WE, et al. F508 CFTR interactome remodelling promotes rescue of cystic fibrosis. *Nature*. 2015; 528(7583):510–6. Epub 2015/12/01. nature15729 [pii] doi: [10.1038/nature15729](https://doi.org/10.1038/nature15729) PMID: [26618866](https://pubmed.ncbi.nlm.nih.gov/26618866/).
31. Trzcinska-Daneluti AM, Chen A, Nguyen L, Murchie R, Jiang C, Moffat J, et al. RNA interference screen to identify kinases that suppress rescue of deltaF508-CFTR. *Mol Cell Proteomics*. 2015. Epub 2015/04/01. M114.046375 [pii] doi: [10.1074/mcp.M114.046375](https://doi.org/10.1074/mcp.M114.046375) PMID: [25825526](https://pubmed.ncbi.nlm.nih.gov/25825526/).
32. Roth DM, Hutt DM, Tong J, Bouchecareilh M, Wang N, Seeley T, et al. Modulation of the maladaptive stress response to manage diseases of protein folding. *PLoS Biol*. 2014; 12(11):e1001998. Epub 2014/11/19. doi: [10.1371/journal.pbio.1001998](https://doi.org/10.1371/journal.pbio.1001998) PBIOLGY-D-14-01135 [pii]. PMID: [25406061](https://pubmed.ncbi.nlm.nih.gov/25406061/); PubMed Central PMCID: PMC4236052.
33. Teem JL, Berger HA, Ostedgaard LS, Rich DP, Tsui LC, Welsh MJ. Identification of revertants for the cystic fibrosis delta F508 mutation using STE6-CFTR chimeras in yeast. *Cell*. 1993; 73(2):335–46. Epub 1993/04/23. 0092-8674(93)90233-G [pii]. PMID: [7682896](https://pubmed.ncbi.nlm.nih.gov/7682896/).
34. Paddon C, Loayza D, Vangelista L, Solari R, Michaelis S. Analysis of the localization of STE6/CFTR chimeras in a *Saccharomyces cerevisiae* model for the cystic fibrosis defect CFTR delta F508. *Mol Microbiol*. 1996; 19(5):1007–17. Epub 1996/03/01. PMID: [8830258](https://pubmed.ncbi.nlm.nih.gov/8830258/).
35. Katzmann DJ, Epping EA, Moye-Rowley WS. Mutational disruption of plasma membrane trafficking of *Saccharomyces cerevisiae* Yor1p, a homologue of mammalian multidrug resistance protein. *Mol Cell Biol*. 1999; 19(4):2998–3009. PMID: [10082567](https://pubmed.ncbi.nlm.nih.gov/10082567/).
36. Pagant S, Halliday JJ, Kougentakis C, Miller EA. Intragenic suppressing mutations correct the folding and intracellular traffic of misfolded mutants of Yor1p, a eukaryotic drug transporter. *J Biol Chem*. 2010; 285(47):36304–14. Epub 2010/09/15. M110.142760 [pii] doi: [10.1074/jbc.M110.142760](https://doi.org/10.1074/jbc.M110.142760) PMID: [20837481](https://pubmed.ncbi.nlm.nih.gov/20837481/); PubMed Central PMCID: PMC2978558.
37. Louie RJ, Guo J, Rodgers JW, White R, Shah N, Pagant S, et al. A yeast phenomic model for the gene interaction network modulating CFTR- Δ F508 protein biogenesis. *Genome Med*. 2012; 4(12):103. doi: [10.1186/gm404](https://doi.org/10.1186/gm404) PMID: [23270647](https://pubmed.ncbi.nlm.nih.gov/23270647/); PubMed Central PMCID: PMC3906889.
38. Winzeler EA, Shoemaker DD, Astromoff A, Liang H, Anderson K, Andre B, et al. Functional characterization of the *S. cerevisiae* genome by gene deletion and parallel analysis. *Science*. 1999; 285(5429):901–6. PMID: [10436161](https://pubmed.ncbi.nlm.nih.gov/10436161/).
39. Louie RJ, Guo J, Rodgers JW, White R, Shah N, Pagant S, et al. A yeast phenomic model for the gene interaction network modulating CFTR-DeltaF508 protein biogenesis. *Genome Med*. 2012; 4(12):103. Epub 2012/12/29. gm404 [pii] doi: [10.1186/gm404](https://doi.org/10.1186/gm404) PMID: [23270647](https://pubmed.ncbi.nlm.nih.gov/23270647/); PubMed Central PMCID: PMC3906889.
40. Treusch S, Hamamichi S, Goodman JL, Matlack KE, Chung CY, Baru V, et al. Functional links between Abeta toxicity, endocytic trafficking, and Alzheimer's disease risk factors in yeast. *Science*. 2011; 334(6060):1241–5. Epub 2011/10/29. doi: [10.1126/science.1213210](https://doi.org/10.1126/science.1213210) science.1213210 [pii]. PMID: [22033521](https://pubmed.ncbi.nlm.nih.gov/22033521/); PubMed Central PMCID: PMC3281757.
41. Tardiff DF, Jui NT, Khurana V, Tambe MA, Thompson ML, Chung CY, et al. Yeast reveal a "drug-gable" Rsp5/Nedd4 network that ameliorates alpha-synuclein toxicity in neurons. *Science*. 2013; 342(6161):979–83. doi: [10.1126/science.1245321](https://doi.org/10.1126/science.1245321) PMID: [24158909](https://pubmed.ncbi.nlm.nih.gov/24158909/); PubMed Central PMCID: PMC3993916.
42. Khurana V, Lindquist S. Modelling neurodegeneration in *Saccharomyces cerevisiae*: why cook with baker's yeast? *Nat Rev Neurosci*. 2010; 11(6):436–49. doi: [10.1038/nrn2809](https://doi.org/10.1038/nrn2809) PMID: [20424620](https://pubmed.ncbi.nlm.nih.gov/20424620/).
43. Huang da W, Sherman BT, Lempicki RA. Bioinformatics enrichment tools: paths toward the comprehensive functional analysis of large gene lists. *Nucleic Acids Res*. 2009; 37(1):1–13. Epub 2008/11/27. gkn923 [pii] doi: [10.1093/nar/gkn923](https://doi.org/10.1093/nar/gkn923) PMID: [19033363](https://pubmed.ncbi.nlm.nih.gov/19033363/); PubMed Central PMCID: PMC2615629.

44. Singh I, Pass R, Togay SO, Rodgers JW, Hartman JLt. Stringent Mating-Type-Regulated Auxotrophy Increases the Accuracy of Systematic Genetic Interaction Screens with *Saccharomyces cerevisiae* Mutant Arrays. *Genetics*. 2009; 181(1):289–300. PMID: [18957706](#); PubMed Central PMCID: PMC2621176. doi: [10.1534/genetics.108.092981](#)
45. Tong AH, Boone C. Synthetic genetic array analysis in *Saccharomyces cerevisiae*. *Methods Mol Biol*. 2006; 313:171–92. PMID: [16118434](#).
46. Shah NA, Laws RJ, Wardman B, Zhao LP, Hartman JLt. Accurate, precise modeling of cell proliferation kinetics from time-lapse imaging and automated image analysis of agar yeast culture arrays. *BMC Syst Biol*. 2007; 1:3. Epub 2007/04/06. 1752-0509-1-3 [pii] doi: [10.1186/1752-0509-1-3](#) PMID: [17408510](#); PubMed Central PMCID: PMC1847469.
47. Ehrhardt C, Collnot EM, Baldes C, Becker U, Laue M, Kim KJ, et al. Towards an in vitro model of cystic fibrosis small airway epithelium: characterisation of the human bronchial epithelial cell line CFBE41o. *Cell Tissue Res*. 2006; 323(3):405–15. Epub 2005/10/27. doi: [10.1007/s00441-005-0062-7](#) PMID: [16249874](#).
48. Veit G, Bossard F, Goepp J, Verkman AS, Galiotta LJ, Hanrahan JW, et al. Proinflammatory cytokine secretion is suppressed by TMEM16A or CFTR channel activity in human cystic fibrosis bronchial epithelia. *Mol Biol Cell*. 2012; 23(21):4188–202. Epub 2012/09/14. mbc.E12-06-0424 [pii] doi: [10.1091/mbc.E12-06-0424](#) PMID: [22973054](#); PubMed Central PMCID: PMC3484098.
49. Sharma M, Pampinella F, Nemes C, Benharouga M, So J, Du K, et al. Misfolding diverts CFTR from recycling to degradation: quality control at early endosomes. *J Cell Biol*. 2004; 164(6):923–33. PMID: [15007060](#).
50. Gluzman R, Okiyoneda T, Mulvihill CM, Rini JM, Barriere H, Lukacs GL. N-glycans are direct determinants of CFTR folding and stability in secretory and endocytic membrane traffic. *J Cell Biol*. 2009; 184(6):847–62. PMID: [19307599](#). doi: [10.1083/jcb.200808124](#)
51. Rowe SM, Pyle LC, Jurkevante A, Varga K, Collawn J, Sloane PA, et al. DeltaF508 CFTR processing correction and activity in polarized airway and non-airway cell monolayers. *Pulm Pharmacol Ther*. 2010; 23(4):268–78. Epub 2010/03/17. S1094-5539(10)00017-9 [pii] doi: [10.1016/j.pupt.2010.02.001](#) PMID: [20226262](#); PubMed Central PMCID: PMC2885545.
52. Bebok Z, Collawn JF, Wakefield J, Parker W, Li Y, Varga K, et al. Failure of cAMP agonists to activate rescued deltaF508 CFTR in CFBE41o- airway epithelial monolayers. *J Physiol*. 2005; 569(Pt 2):601–15. Epub 2005/10/08. jphysiol.2005.096669 [pii] doi: [10.1113/jphysiol.2005.096669](#) PMID: [16210354](#); PubMed Central PMCID: PMC1464253.
53. Ramachandran S, Krishnamurthy S, Jacobi AM, Wohlford-Lenane C, Behlke MA, Davidson BL, et al. Efficient delivery of RNA interference oligonucleotides to polarized airway epithelia in vitro. *Am J Physiol Lung Cell Mol Physiol*. 2013; 305(1):L23–32. Epub 2013/04/30. ajplung.00426.2012 [pii] doi: [10.1152/ajplung.00426.2012](#) PMID: [23624792](#); PubMed Central PMCID: PMC4073929.
54. Van Goor F, Hadida S, Grootenhuys PD, Burton B, Stack JH, Straley KS, et al. Correction of the F508del-CFTR protein processing defect in vitro by the investigational drug VX-809. *Proc Natl Acad Sci U S A*. 2011; 108(46):18843–8. PMID: [21976485](#). doi: [10.1073/pnas.1105787108](#)
55. Apaja PM, Foo B, Okiyoneda T, Valinsky WC, Barriere H, Atanasiu R, et al. Ubiquitination-dependent quality control of hERG K⁺ channel with acquired and inherited conformational defect at the plasma membrane. *Mol Biol Cell*. 2013; 24(24):3787–804. Epub 2013/10/25. mbc.E13-07-0417 [pii] doi: [10.1091/mbc.E13-07-0417](#) PMID: [24152733](#).
56. Apaja PM, Xu H, Lukacs GL. Quality control for unfolded proteins at the plasma membrane. *J Cell Biol*. 2010; 191(3):553–70. Epub 2010/10/27. jcb.201006012 [pii] doi: [10.1083/jcb.201006012](#) PMID: [20974815](#).
57. Takahashi K, Makita N, Manaka K, Hisano M, Akioka Y, Miura K, et al. V2 vasopressin receptor (V2R) mutations in partial nephrogenic diabetes insipidus highlight protean agonism of V2R antagonists. *J Biol Chem*. 2012; 287(3):2099–106. Epub 2011/12/07. M111.268797 [pii] doi: [10.1074/jbc.M111.268797](#) PMID: [22144672](#); PubMed Central PMCID: PMC3265889.
58. Duarri A, Teijido O, Lopez-Hernandez T, Scheper GC, Barriere H, Boor I, et al. Molecular pathogenesis of megalencephalic leukoencephalopathy with subcortical cysts: mutations in MLC1 cause folding defects. *Hum Mol Genet*. 2008; 17(23):3728–39. Epub 2008/09/02. ddn269 [pii] doi: [10.1093/hmg/ddn269](#) PMID: [18757878](#); PubMed Central PMCID: PMC2581428.
59. Keating MT, Sanguinetti MC. Molecular and cellular mechanisms of cardiac arrhythmias. *Cell*. 2001; 104(4):569–80. Epub 2001/03/10. S0092-8674(01)00243-4 [pii]. PMID: [11239413](#).
60. Anderson CL, Delisle BP, Anson BD, Kilby JA, Will ML, Tester DJ, et al. Most LQT2 mutations reduce Kv11.1 (hERG) current by a class 2 (trafficking-deficient) mechanism. *Circulation*. 2006; 113(3):365–73. Epub 2006/01/25. 113/3/365 [pii] doi: [10.1161/CIRCULATIONAHA.105.570200](#) PMID: [16432067](#).

61. Ficker E, Dennis AT, Wang L, Brown AM. Role of the cytosolic chaperones Hsp70 and Hsp90 in maturation of the cardiac potassium channel HERG. *Circ Res.* 2003; 92(12):e87–100. Epub 2003/05/31. doi: [10.1161/01.RES.0000079028.31393.1501](https://doi.org/10.1161/01.RES.0000079028.31393.1501) RES.0000079028.31393.15 [pii]. PMID: [12775586](https://pubmed.ncbi.nlm.nih.gov/12775586/).
62. Tsai CJ, Sauna ZE, Kimchi-Sarfaty C, Ambudkar SV, Gottesman MM, Nussinov R. Synonymous mutations and ribosome stalling can lead to altered folding pathways and distinct minima. *J Mol Biol.* 2008; 383(2):281–91. Epub 2008/08/30. S0022-2836(08)00992-3 [pii] doi: [10.1016/j.jmb.2008.08.012](https://doi.org/10.1016/j.jmb.2008.08.012) PMID: [18722384](https://pubmed.ncbi.nlm.nih.gov/18722384/); PubMed Central PMCID: [PMC2628389](https://pubmed.ncbi.nlm.nih.gov/PMC2628389/).
63. Spencer PS, Siller E, Anderson JF, Barral JM. Silent substitutions predictably alter translation elongation rates and protein folding efficiencies. *J Mol Biol.* 2012; 422(3):328–35. Epub 2012/06/19. S0022-2836(12)00483-4 [pii] doi: [10.1016/j.jmb.2012.06.010](https://doi.org/10.1016/j.jmb.2012.06.010) PMID: [22705285](https://pubmed.ncbi.nlm.nih.gov/22705285/); PubMed Central PMCID: [PMC3576719](https://pubmed.ncbi.nlm.nih.gov/PMC3576719/).
64. Kimchi-Sarfaty C, Oh JM, Kim IW, Sauna ZE, Calcagno AM, Ambudkar SV, et al. A "silent" polymorphism in the MDR1 gene changes substrate specificity. *Science.* 2007; 315(5811):525–8. Epub 2006/12/23. 1135308 [pii] doi: [10.1126/science.1135308](https://doi.org/10.1126/science.1135308) PMID: [17185560](https://pubmed.ncbi.nlm.nih.gov/17185560/).
65. Morgunov AS, Babu MM. Optimizing membrane-protein biogenesis through nonoptimal-codon usage. *Nat Struct Mol Biol.* 2014; 21(12):1023–5. Epub 2014/12/04. nsmb.2926 [pii] doi: [10.1038/nsmb.2926](https://doi.org/10.1038/nsmb.2926) PMID: [25469841](https://pubmed.ncbi.nlm.nih.gov/25469841/).
66. Sharma M, Benharouga M, Hu W, Lukacs GL. Conformational and temperature-sensitive stability defects of the delta F508 cystic fibrosis transmembrane conductance regulator in post-endoplasmic reticulum compartments. *J Biol Chem.* 2001; 276(12):8942–50. PMID: [11124952](https://pubmed.ncbi.nlm.nih.gov/11124952/).
67. Briones E, Briones C, Remacha M, Ballesta JP. The GTPase center protein L12 is required for correct ribosomal stalk assembly but not for *Saccharomyces cerevisiae* viability. *J Biol Chem.* 1998; 273(48):31956–61. Epub 1998/11/21. PMID: [9822666](https://pubmed.ncbi.nlm.nih.gov/9822666/).
68. Steffen KK, McCormick MA, Pham KM, MacKay VL, Delaney JR, Murakami CJ, et al. Ribosome deficiency protects against ER stress in *Saccharomyces cerevisiae*. *Genetics.* 2012; 191(1):107–18. Epub 2012/03/02. genetics.111.136549 [pii] doi: [10.1534/genetics.111.136549](https://doi.org/10.1534/genetics.111.136549) PMID: [22377630](https://pubmed.ncbi.nlm.nih.gov/22377630/); PubMed Central PMCID: [PMC3338253](https://pubmed.ncbi.nlm.nih.gov/PMC3338253/).
69. Ingolia NT, Lareau LF, Weissman JS. Ribosome profiling of mouse embryonic stem cells reveals the complexity and dynamics of mammalian proteomes. *Cell.* 2011; 147(4):789–802. Epub 2011/11/08. S0092-8674(11)01192-5 [pii] doi: [10.1016/j.cell.2011.10.002](https://doi.org/10.1016/j.cell.2011.10.002) PMID: [22056041](https://pubmed.ncbi.nlm.nih.gov/22056041/); PubMed Central PMCID: [PMC3225288](https://pubmed.ncbi.nlm.nih.gov/PMC3225288/).
70. Fresno M, Jimenez A, Vazquez D. Inhibition of translation in eukaryotic systems by harringtonine. *Eur J Biochem.* 1977; 72(2):323–30. Epub 1977/01/01. PMID: [319998](https://pubmed.ncbi.nlm.nih.gov/319998/).
71. Schneider-Poetsch T, Ju J, Eyler DE, Dang Y, Bhat S, Merrick WC, et al. Inhibition of eukaryotic translation elongation by cycloheximide and lactimidomycin. *Nat Chem Biol.* 2010; 6(3):209–17. Epub 2010/02/02. nchembio.304 [pii] doi: [10.1038/nchembio.304](https://doi.org/10.1038/nchembio.304) PMID: [20118940](https://pubmed.ncbi.nlm.nih.gov/20118940/); PubMed Central PMCID: [PMC2831214](https://pubmed.ncbi.nlm.nih.gov/PMC2831214/).
72. Meriin AB, Mense M, Colbert JD, Liang F, Bihler H, Zaarur N, et al. A novel approach to recovery of function of mutant proteins by slowing down translation. *J Biol Chem.* 2012; 287(41):34264–72. Epub 2012/08/21. M112.397307 [pii] doi: [10.1074/jbc.M112.397307](https://doi.org/10.1074/jbc.M112.397307) PMID: [22902621](https://pubmed.ncbi.nlm.nih.gov/22902621/); PubMed Central PMCID: [PMC3464534](https://pubmed.ncbi.nlm.nih.gov/PMC3464534/).
73. Francisco-Velilla R, Remacha M, Ballesta JP. Carboxy terminal modifications of the P0 protein reveal alternative mechanisms of nuclear ribosomal stalk assembly. *Nucleic Acids Res.* 2013; 41(18):8628–36. Epub 2013/07/25. gkt637 [pii] doi: [10.1093/nar/gkt637](https://doi.org/10.1093/nar/gkt637) PMID: [23880660](https://pubmed.ncbi.nlm.nih.gov/23880660/); PubMed Central PMCID: [PMC3794597](https://pubmed.ncbi.nlm.nih.gov/PMC3794597/).
74. Gonzalo P, Reboud JP. The puzzling lateral flexible stalk of the ribosome. *Biol Cell.* 2003; 95(3–4):179–93. Epub 2003/07/18. S0248490003000340 [pii]. PMID: [12867082](https://pubmed.ncbi.nlm.nih.gov/12867082/).
75. Jimenez-Diaz A, Remacha M, Ballesta JP, Berlanga JJ. Phosphorylation of initiation factor eIF2 in response to stress conditions is mediated by acidic ribosomal P1/P2 proteins in *Saccharomyces cerevisiae*. *PLoS One.* 2013; 8(12):e84219. Epub 2014/01/07. doi: [10.1371/journal.pone.0084219](https://doi.org/10.1371/journal.pone.0084219) PONE-D-13-28530 [pii]. PMID: [24391917](https://pubmed.ncbi.nlm.nih.gov/24391917/); PubMed Central PMCID: [PMC3877244](https://pubmed.ncbi.nlm.nih.gov/PMC3877244/).
76. Bargis-Surgey P, Lavergne JP, Gonzalo P, Vard C, Filhol-Cochet O, Reboud JP. Interaction of elongation factor eEF-2 with ribosomal P proteins. *Eur J Biochem.* 1999; 262(2):606–11. Epub 1999/05/21. PMID: [10336649](https://pubmed.ncbi.nlm.nih.gov/10336649/).
77. Stark H, Rodnina MV, Rinke-Appel J, Brimacombe R, Wintermeyer W, van Heel M. Visualization of elongation factor Tu on the *Escherichia coli* ribosome. *Nature.* 1997; 389(6649):403–6. Epub 1997/10/06. doi: [10.1038/38770](https://doi.org/10.1038/38770) PMID: [9311785](https://pubmed.ncbi.nlm.nih.gov/9311785/).
78. Schekman R. Lasker Basic Medical Research Award. SEC mutants and the secretory apparatus. *Nat Med.* 2002; 8(10):1055–8. Epub 2002/10/03. doi: [10.1038/nm769](https://doi.org/10.1038/nm769) nm769 [pii]. PMID: [12357231](https://pubmed.ncbi.nlm.nih.gov/12357231/).

79. Hartman JLT, Garvik B, Hartwell L. Principles for the buffering of genetic variation. *Science*. 2001; 291(5506):1001–4. Epub 2001/03/10. PMID: [11232561](#).
80. Hartman JLT, Stisher C, Outlaw DA, Guo J, Shah NA, Tian D, et al. Yeast Phenomics: An Experimental Approach for Modeling Gene Interaction Networks that Buffer Disease. *Genes (Basel)*. 2015; 6(1):24–45. Epub 2015/02/11. genes6010024 [pii] doi: [10.3390/genes6010024](#) PMID: [25668739](#); PubMed Central PMCID: PMC4377832.
81. Wolfe KH, Shields DC. Molecular evidence for an ancient duplication of the entire yeast genome. *Nature*. 1997; 387(6634):708–13. Epub 1997/06/12. doi: [10.1038/42711](#) PMID: [9192896](#).
82. O'Brien EP, Ciryam P, Vendruscolo M, Dobson CM. Understanding the influence of codon translation rates on cotranslational protein folding. *Acc Chem Res*. 2014; 47(5):1536–44. Epub 2014/05/03. doi: [10.1021/ar5000117](#) PMID: [24784899](#).
83. Nissley DA, Sharma AK, Ahmed N, Friedrich UA, Kramer G, Bukau B, et al. Accurate prediction of cellular co-translational folding indicates proteins can switch from post- to co-translational folding. *Nat Commun*. 2016; 7:10341. Epub 2016/02/19. ncomms10341 [pii] doi: [10.1038/ncomms10341](#) PMID: [26887592](#); PubMed Central PMCID: PMC4759629.
84. Kaiser CM, Goldman DH, Chodera JD, Tinoco I Jr., Bustamante C. The ribosome modulates nascent protein folding. *Science*. 2011; 334(6063):1723–7. Epub 2011/12/24. 334/6063/1723 [pii] doi: [10.1126/science.1209740](#) PMID: [22194581](#); PubMed Central PMCID: PMC4172366.
85. O'Brien EP, Christodoulou J, Vendruscolo M, Dobson CM. New scenarios of protein folding can occur on the ribosome. *J Am Chem Soc*. 2011; 133(3):513–26. Epub 2011/01/06. doi: [10.1021/ja107863z](#) PMID: [21204555](#).
86. Kosolapov A, Deutsch C. Tertiary interactions within the ribosomal exit tunnel. *Nat Struct Mol Biol*. 2009; 16(4):405–11. Epub 2009/03/10. nsmb.1571 [pii] doi: [10.1038/nsmb.1571](#) PMID: [19270700](#); PubMed Central PMCID: PMC2670549.
87. Kramer G, Boehringer D, Ban N, Bukau B. The ribosome as a platform for co-translational processing, folding and targeting of newly synthesized proteins. *Nat Struct Mol Biol*. 2009; 16(6):589–97. Epub 2009/06/06. nsmb.1614 [pii] doi: [10.1038/nsmb.1614](#) PMID: [19491936](#).
88. Pechmann S, Chartron JW, Frydman J. Local slowdown of translation by nonoptimal codons promotes nascent-chain recognition by SRP in vivo. *Nat Struct Mol Biol*. 2014; 21(12):1100–5. Epub 2014/11/25. nsmb.2919 [pii] doi: [10.1038/nsmb.2919](#) PMID: [25420103](#).
89. Kim SJ, Yoon JS, Shishido H, Yang Z, Rooney LA, Barral JM, et al. Protein folding. Translational tuning optimizes nascent protein folding in cells. *Science*. 2015; 348(6233):444–8. Epub 2015/04/25. 348/6233/444 [pii] doi: [10.1126/science.aaa3974](#) PMID: [25908822](#).
90. Zhou M, Guo J, Cha J, Chae M, Chen S, Barral JM, et al. Non-optimal codon usage affects expression, structure and function of clock protein FRQ. *Nature*. 2013; 495(7439):111–5. Epub 2013/02/19. nature11833 [pii] doi: [10.1038/nature11833](#) PMID: [23417067](#); PubMed Central PMCID: PMC3629845.
91. Kartner N, Augustinas O, Jensen TJ, Naismith AL, Riordan JR. Mislocalization of delta F508 CFTR in cystic fibrosis sweat gland. *Nat Genet*. 1992; 1(5):321–7. Epub 1992/08/01. doi: [10.1038/ng0892-321](#) PMID: [1284548](#).
92. Spahn CM, Gomez-Lorenzo MG, Grassucci RA, Jorgensen R, Andersen GR, Beckmann R, et al. Domain movements of elongation factor eEF2 and the eukaryotic 80S ribosome facilitate tRNA translocation. *EMBO J*. 2004; 23(5):1008–19. Epub 2004/02/21. doi: [10.1038/sj.emboj.7600102](#) 7600102 [pii] PMID: [14976550](#); PubMed Central PMCID: PMC380967.
93. Anger AM, Armache JP, Berninghausen O, Habeck M, Subklewe M, Wilson DN, et al. Structures of the human and Drosophila 80S ribosome. *Nature*. 2013; 497(7447):80–5. Epub 2013/05/03. nature12104 [pii] doi: [10.1038/nature12104](#) PMID: [23636399](#).
94. Ito K, Honda T, Suzuki T, Miyoshi T, Murakami R, Yao M, et al. Molecular insights into the interaction of the ribosomal stalk protein with elongation factor 1alpha. *Nucleic Acids Res*. 2014; 42(22):14042–52. Epub 2014/11/28. gku1248 [pii] doi: [10.1093/nar/gku1248](#) PMID: [25428348](#); PubMed Central PMCID: PMC4267659.
95. Briceno V, Camargo H, Remacha M, Santos C, Ballesta JP. Structural and functional characterization of the amino terminal domain of the yeast ribosomal stalk P1 and P2 proteins. *Int J Biochem Cell Biol*. 2009; 41(6):1315–22. Epub 2008/12/17. S1357-2725(08)00479-2 [pii] doi: [10.1016/j.biocel.2008.11.005](#) PMID: [19084076](#).
96. Krokowski D, Boguszewska A, Abramczyk D, Liljas A, Tchorzewski M, Grankowski N. Yeast ribosomal P0 protein has two separate binding sites for P1/P2 proteins. *Mol Microbiol*. 2006; 60(2):386–400. Epub 2006/04/01. MMI5117 [pii] doi: [10.1111/j.1365-2958.2006.05117.x](#) PMID: [16573688](#).
97. Remacha M, Jimenez-Diaz A, Bermejo B, Rodriguez-Gabriel MA, Guarinos E, Ballesta JP. Ribosomal acidic phosphoproteins P1 and P2 are not required for cell viability but regulate the pattern of protein

- expression in *Saccharomyces cerevisiae*. *Mol Cell Biol*. 1995; 15(9):4754–62. Epub 1995/09/01. PMID: [7651393](#); PubMed Central PMCID: PMC230719.
98. Griesenbach U, Geddes DM, Alton EW. The pathogenic consequences of a single mutated CFTR gene. *Thorax*. 1999; 54 Suppl 2:S19–23. Epub 1999/08/19. PMID: [10451687](#); PubMed Central PMCID: PMC1765929.
 99. Van Goor F, Hadida S, Grootenhuys PD, Burton B, Cao D, Neuberger T, et al. Rescue of CF airway epithelial cell function in vitro by a CFTR potentiator, VX-770. *Proc Natl Acad Sci U S A*. 2009; 106(44):18825–30. PMID: [19846789](#). doi: [10.1073/pnas.0904709106](#)
 100. Neuberger T, Burton B, Clark H, Van Goor F. Use of primary cultures of human bronchial epithelial cells isolated from cystic fibrosis patients for the pre-clinical testing of CFTR modulators. *Methods Mol Biol*. 2011; 741:39–54. Epub 2011/05/20. doi: [10.1007/978-1-61779-117-8_4](#) PMID: [21594777](#).
 101. Liu L, Chu KK, Houser GH, Diephuis BJ, Li Y, Wilsterman EJ, et al. Method for quantitative study of airway functional microanatomy using micro-optical coherence tomography. *PLoS One*. 2013; 8(1):e54473. Epub 2013/02/02. doi: [10.1371/journal.pone.0054473](#) PONE-D-12-31290 [pii]. PMID: [23372732](#); PubMed Central PMCID: PMC3553101.
 102. Liu X, Ory V, Chapman S, Yuan H, Albanese C, Kallakury B, et al. ROCK inhibitor and feeder cells induce the conditional reprogramming of epithelial cells. *Am J Pathol*. 2012; 180(2):599–607. Epub 2011/12/23. S0002-9440(11)01059-5 [pii] doi: [10.1016/j.ajpath.2011.10.036](#) PMID: [22189618](#); PubMed Central PMCID: PMC3349876.
 103. Hutt DM, Herman D, Rodrigues AP, Noel S, Pilewski JM, Matteson J, et al. Reduced histone deacetylase 7 activity restores function to misfolded CFTR in cystic fibrosis. *Nat Chem Biol*. 2010; 6(1):25–33. Epub 2009/12/08. nchembio.275 [pii] doi: [10.1038/nchembio.275](#) PMID: [19966789](#); PubMed Central PMCID: PMC2901172.
 104. Rabeh WM, Bossard F, Xu H, Okiyoneda T, Bagdany M, Mulvihill CM, et al. Correction of both NBD1 energetics and domain interface is required to restore Δ F508 CFTR folding and function. *Cell*. 2012; 148(1–2):150–63. Epub 2012/01/24. S0092-8674(11)01368-7 [pii] doi: [10.1016/j.cell.2011.11.024](#) PMID: [22265408](#); PubMed Central PMCID: PMC3431169.